The Plant Cell, Vol. 26: 3792–3808, September 2014, www.plantcell.org

Multiple *N*-Glycans Cooperate in the Subcellular Targeting and Functioning of *Arabidopsis* KORRIGAN1[W]

Stephan Rips,[a] Nolan Bentley,[b] In Sil Jeong,[b] Justin L. Welch,[b] Antje von Schaewen,[a,1] and Hisashi Koiwa[b,1,2]

[a] Institut für Biologie und Biotechnologie der Pflanzen, Westfälische Wilhelms-Universität Münster, 48149 Münster, Germany
[b] Vegetable and Fruit Improvement Center, Department of Horticultural Sciences, Molecular and Environmental Plant Science Program, Texas A&M University, College Station, Texas 77843-2133

ORCID ID: 0000-0002-7421-340X (H.K.)

Arabidopsis thaliana **KORRIGAN1 (KOR1) is an integral membrane endo-β1,4-glucanase in the *trans*-Golgi network and plasma membrane that is essential for cellulose biosynthesis. The extracellular domain of KOR1 contains eight *N*-glycosylation sites, N1 to N8, of which only N3 to N7 are highly conserved. Genetic evidence indicated that cellular defects in attachment and maturation of these *N*-glycans affect KOR1 function in vivo, whereas the manner by which *N*-glycans modulate KOR1 function remained obscure. Site-directed mutagenesis analysis of green fluorescent protein (GFP)-KOR1 expressed from its native regulatory sequences established that all eight *N*-glycosylation sites (N1 to N8) are used in the wild type, whereas *stt3a-2* cells could only inefficiently add *N*-glycans to less conserved sites. GFP-KOR1 variants with a single *N*-glycan at nonconserved sites were less effective than those with one at a highly conserved site in rescuing the root growth phenotype of *rsw2-1* (*kor1* allele). When functionally compromised, GFP-KOR1 tended to accumulate at the tonoplast. GFP-KOR1Δall (without any *N*-glycan) exhibited partial complementation of *rsw2-1*; however, root growth of this line was still negatively affected by the absence of complex-type *N*-glycan modifications in the host plants. These results suggest that one or several additional factor(s) carrying complex *N*-glycans cooperate(s) with KOR1 in *trans* to grant proper targeting/functioning in plant cells.**

INTRODUCTION

In plants, many cell surface receptors and cell wall proteins are decorated with multiple *N*-linked glycans (*N*-glycans). Eukaryotic *N*-glycosylation may occur co- and posttranslationally on proteins that are residents of or migrate through the secretory pathway. When a glycoprotein precursor enters the luminal space of the endoplasmic reticulum (ER), oligosaccharyltransferase (OST), a multisubunit enzyme complex (Silberstein and Gilmore, 1996; Helenius and Aebi, 2001) transfers *core* oligosaccharides ($Glc_3Man_9GlcNac_2$) preassembled on membrane-linked dolicholpyrophosphate to certain asparagine residues (Asn-X-Ser/Thr, NXS/T motif) within the nascent polypeptide chain. Central to this complex is the STT3 (STAUROSPORIN AND TEMPERATURE SENSITIVE3) subunit, which is responsible for recognizing the NXS/T motif and for the transfer reaction. Higher eukaryotes contain two isoforms of STT3 that are able to conduct cotranslational and posttranslational *N*-glycosylation reactions, respectively (Kelleher et al., 2003). *N*-glycans attached in the ER lumen are important for folding of nascent polypeptides because they recruit the lectin chaperones calnexin and calreticulin during ER quality control cycles (ERQC) (Oliver et al., 1997). Successfully folded glycoproteins are exported to the Golgi apparatus (GA), whereas proteins that fail to adopt their native conformation after multiple rounds of folding attempts are destroyed by an ER-associated degradation pathway (Vembar and Brodsky, 2008).

In higher eukaryotes, glycosidases and glycosyltransferases in the GA are responsible for the formation of intermediate hybrid *N*-glycans and mature complex-type *N*-glycans (Varki, 2011). Complex *N*-glycans of plants are unique because they contain *core* α1,3-fucose and β1,2-xylose residues that are not found in mammalian and human *N*-glycans (Johnson and Chrispeels, 1987; Laurière et al., 1989). High mannose *N*-glycans on glycoproteins exported from the ER are initially trimmed by α-mannosidase I in the *cis*-Golgi (Liebminger et al., 2009; Kajiura et al., 2010). The first committed step in the formation of complex *N*-glycans in the GA is catalyzed by β1,2-*N*-acetylglucosaminyltransferase I (GlcNac transferase I [GnTI]) (von Schaewen et al., 1993) and is followed by steps catalyzed by α-mannosidase II (Strasser et al., 2006), β1,2-*N*-acetylglucosaminyltransferase II (GnTII) (Strasser et al., 1999), β1,2-xylosyltransferase (Strasser et al., 2000), and α1,3-fucosyltransferase (Strasser et al., 2004). The two terminal GlcNac residues of some *N*-glycans are further modified by β1,3-galactosyltransferase (Strasser et al., 2007b) and α1,4-fucosyltransferase (Léonard et al., 2002) to produce Lewis a epitopes (Fitchette-Lainé et al., 1997), whereas the terminal GlcNac residues of most *N*-glycans are trimmed by hexosaminidases in the apoplast and vacuoles, resulting in paucimannosidic $Man_3XylFucGlcNac_2$ structures (Strasser et al., 2007a; Liebminger et al., 2011). In *Arabidopsis thaliana*, about three quarters (73.9%) of all *N*-linked glycans are converted to complex-types. Of the complex *N*-glycans, about half (36.0% and 35.7%, or 26.6 and 26.4% of total *N*-glycans) are GlcNac-terminated or fully trimmed, displaying the structure $GlcNac_2Man_3XylFucGlcNac_2$ or $Man_3XylFucGlcNac_2$, respectively (Strasser et al., 2004).

[1] These authors contributed equally to this work.
[2] Address correspondence to koiwa@tamu.edu.
The authors responsible for distribution of materials integral to the findings presented in this article in accordance with the policy described in the Instructions for Authors (www.plantcell.org) are: Antje von Schaewen (schaewen@uni-muenster.de) and Hisashi Koiwa (koiwa@tamu.edu).
[W] Online version contains Web-only data.
www.plantcell.org/cgi/doi/10.1105/tpc.114.129718

In mammals, mutations that compromise the *N*-glycan modification pathway in the GA are associated with type-II congenital disorders of glycosylation (Lehle et al., 2006). In plants, however, salt-sensitive root growth has been the only clear phenotype associated with mutations of the *N*-glycan modification pathway in the GA (Kang et al., 2008). Data obtained from genetic interaction analyses suggest that complex *N*-glycans attached to KORRIGAN1/RADIALLY SWOLLEN2 (KOR1/RSW2) protein are important during the salt stress response (Frank et al., 2008; Kang et al., 2008; von Schaewen et al., 2008). KOR1/RSW2 encodes a type-II transmembrane protein with endo-β1,4-glucanase activity linked to cellulose biosynthesis (Lane et al., 2001; Peng et al., 2002) and has been suggested to function in relieving tension from cellulose microfibrils (Takahashi et al., 2009). Recent studies showed that KOR1 physically interacts and colocalizes with the cellulose synthase complex in vivo (Lei et al., 2014; Vain et al., 2014). As shown previously, *complex glycan-less1* (*cgl1*) mutations affecting GnTI activity in early Golgi cisternae enhance the growth defect of plants carrying the temperature-sensitive *rsw2-1* allele (G429R change) (Lane et al., 2001), even at the permissive temperature (Kang et al., 2008). While the KOR1/RSW2 protein sequence contains eight *N*-glycosylation motifs, of which many are highly conserved among plant homologs, the same protein family (glycoside hydrolase family 9) also contains prokaryotic enzymes that entirely lack protein *N*-glycosylation (Jung et al., 1993; Master et al., 2004). Thus, KOR1/RSW2 provides a unique model to study the requirement of individual *N*-glycans for stability, targeting, and functioning of secretory glycoproteins with multiple *N*-glycosylation sites. Analyses of KOR1 heterologously expressed in insect cells provided some insight into the role of KOR1 *N*-glycans in enzymatic activity (Liebminger et al., 2013); however, the in planta function of individual KOR1 *N*-glycans remained obscure.

Here, we report the systematic characterization of *N*-glycan functionality for KOR1 by stepwise mutagenesis of *N*-glycosylation sites and subsequent complementation analysis in the *rsw2-1* (*kor1*) mutant. We found that, although all eight potential *N*-glycosylation sites are used, loss of single *N*-glycans did not impair KOR1 functions in plant growth. Even combinations of up to six *N*-glycosylation site mutations were tolerated without causing substantial growth defects. However, the sufficiency of individual *N*-glycans varied and correlated with conservation among other plant homologs. The subcellular distribution of underglycosylated KOR1 variants differed from wild-type KOR1, as they were not effectively retained in the *trans*-Golgi network (TGN). Although a KOR1 variant lacking all *N*-glycans (green fluorescent protein [GFP]-KOR1Δall) could weakly complement both *rsw2-1* and the *rsw2-1 cgl1-3* double mutant, lack of complex *N*-glycan formation in *cgl1* still affected the in vivo function of GFP-KOR1Δall. Together, our data indicate that KOR1 harbors both essential and nonessential *N*-glycosylation sites and that essential functions are shared among multiple *N*-glycans. Furthermore, the enhancing effect caused by genetic interaction between *rsw2-1* and *N*-glycan maturation defects in *cgl1-3* seems to be indirect, suggesting that additional glycoprotein factors cooperate with KOR1 during plant growth and stress tolerance.

RESULTS

Identification of Highly Conserved *N*-Glycan Positions on KOR1

The KOR1 polypeptide sequence contains eight *N*-glycosylation motifs within the luminal/extracellular domain (Figure 1A), which are referred to as position N1 through N8 hereafter. When available glycoside hydrolase family 9 sequences were aligned with that of KOR1, we found a varying degree of conservation for each *N*-glycosylation site. A high degree of conservation (94 to 100%) was found for central positions N3 to N7, whereas conservation was low for peripheral positions N1, N2, and N8 (51 to 78%). We used three-dimensional modeling of the extracellular KOR1 domain (based on a homologous termite endo-β1,4-glucanase) (Khademi et al., 2002) for mapping all *N*-glycans attached to the protein backbone. The resulting glycosylated KOR1 domain adopts a coffee bean-shaped structure with the notched side harboring the substrate binding cleft (front) and a dome-shaped backside (Figure 1B). Glycans N1 and N2 are located on the back, whereas glycans N3, N5, N6, and N8 are located at the periphery of the enzyme, projecting themselves in parallel to the surface plane along the catalytic cleft. Glycan N7 lies close to the rim of the substrate binding site and in close proximity to N8 upon folding. Although the program was unable to model glycan N4 at ^{324}N, its *N*-glycosylation site also resides close to the edge of the catalytic cleft facing N7.

Reporter Systems Visualize Expression and Subcellular Localization without Compromising in Vivo Function of KOR1

We hypothesized that subcellular targeting and/or catalytic activity of KOR1 has unique requirements for specific *N*-glycans at different positions. To score the function of KOR1 *N*-glycans in vivo, we prepared a series of complementation constructs that produce KOR1 proteins with altered *N*-glycosylation patterns. These expression cassettes are based on the RGS-His-KOR1 genomic fragment, which was previously used to complement the *irx2-1* allele of KOR1, defective in secondary cell wall formation (Szyjanowicz et al., 2004). For ease of mutagenesis, the coding region was replaced with KOR1 cDNA and, to allow monitoring of gene expression and subcellular localization, β-glucuronidase (GUS)- or GFP-reporter genes were inserted at the 6xHis region within the N-terminal cytoplasmic domain (after amino acid L31), immediately before the 6xHis tag (RG<reporter>S-His) (Supplemental Figure 1A).

The function of the modified KOR1 expression cassettes was tested in planta. The expression profile of wild-type GUS-KOR1 largely confirmed preceding studies of *KOR1*-mRNA expression and overlaps with the GUS expression profile driven by the *Arabidopsis* KOR1 promoter (Takahashi et al., 2009) (Supplemental Figure 1B). The expression pattern of the *GFP-KOR1* construct was similar to that of the *GUS-KOR1* construct, indicating that GFP-tagged KOR1 also mirrors the expression profile of endogenous KOR1. To confirm proper in planta function, the performance of *rsw2-1* transformed with the tagged KOR1 constructs was tested. The *rsw2-1* allele of *KOR1* represents a missense mutation

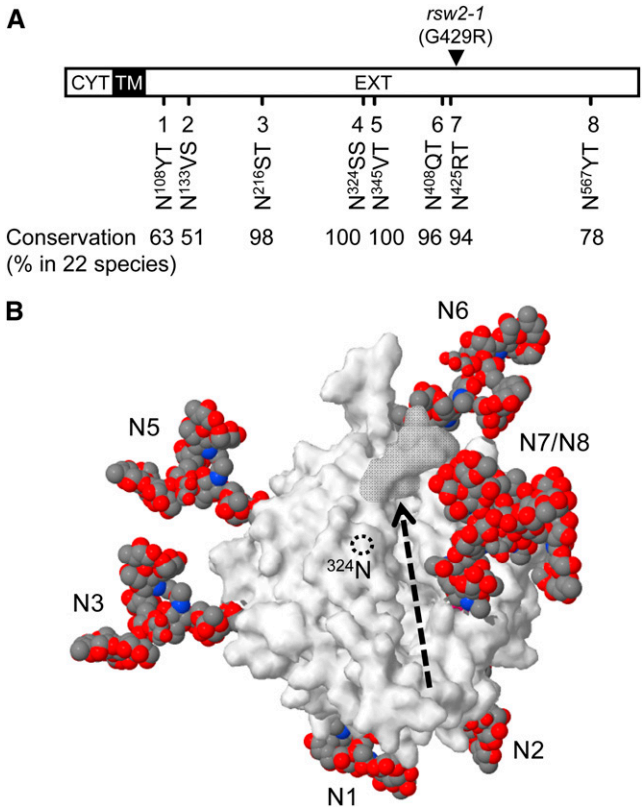

Figure 1. Structure of the KOR1 Protein.

(A) KOR1 consists of a cytoplasmic domain (CYT), a transmembrane domain (TM), and an extracellular (EXT) catalytic domain. Positions of the eight *N*-glycosylation sites (NXT/S) and the G429R point mutation (in *rsw2-1*) are shown to scale (reporters were inserted within the cytoplasmic domain). Percentage (%) of conservation for each *N*-glycosylation site in 52 KOR1 homologs from 22 species is indicated.

(B) Extracellular KOR1 domain (surface mode) with complex *N*-glycans (GlcNac2M3XF, space-fill mode) shown in CPK coloring. The active site cleft (dashed arrow) is limited by the blocking loop (position 359-369) shaded in gray. Note that important E-series glycans N7 and N4 (attached to N^{324}, dotted circle) face each other at the edge of the substrate binding cleft.

that confers temperature sensitivity to KOR1 (Lane et al., 2001) (Figure 1A). As shown in Supplemental Figure 1C, GFP-KOR1 was able to complement the *rsw2-1* mutant phenotype in both roots and shoots. Noteworthy, the extent of complementation by GFP-KOR1 obtained here is higher than that previously reported for a 35S-driven *GFP-KOR1* construct, which showed only partial complementation in roots (Robert et al., 2005). Therefore, the GFP-KOR1 lines were used for further experiments.

GFP-KOR1 Accumulates in the TGN and at the Plasma Membrane

Biochemical studies on the endogenous *Arabidopsis* KOR1 protein have established that KOR1 predominantly resides in the plasma membrane (PM; Nicol et al., 1998) and TGN (Drakakaki et al., 2012). Previous studies using GFP fused to the N or C terminus of KOR1 produced subcellular localization profiles inconsistent with the biochemical studies, i.e., predominant labeling of the cell plate (C-terminally fused GFP; Zuo et al., 2000) or early endosomes/tonoplast (N-terminally fused GFP; Robert et al., 2005). We therefore first validated the authenticity of subcellular localization of the newly prepared GFP-KOR1 fusions by confocal microscopy (Figure 2A) in both Columbia-0 (Col-0) (wild type) and *rsw2-1* (complementation host). The patterns obtained in Col-0 and *rsw2-1* were indistinguishable, indicating that localization of GFP-KOR1 is independent of the functional state of endogenous KOR1. In general, fluorescent signals were observed at the PM and intracellular particles similar to Golgi stacks (~1 μm), with characteristic stop-and-go movements (Nebenführ et al., 1999) close to the cell surface (Figure 2A). To determine the identity of the GFP-labeled structures, GFP-KOR1 was coexpressed in transgenic plants with organelle markers including one each for the ER (BiP-RFP [red fluorescent protein]), the GA (XylT-RFP), and the TGN (SYP61-CFP [cyan fluorescent protein]) (Figures 2B to 2D). Some overlapping/adjacent GFP and RFP signals were observed with GFP-KOR1 and XylT-RFP (GA) (Figure 2C, panel d, arrowheads) but not with GFP-KOR1 and BiP-RFP (ER) (Figure 2B). In plants coexpressing GFP-KOR1 and SYP61-CFP (TGN), clear overlap of GFP and CFP signals was observed (Figure 2D, panel d, arrowheads), albeit only GFP-KOR1 signals were detected at the PM. These results established that KOR1 predominantly localizes to the TGN and PM. In addition, weak GFP-KOR1 signals were often observed at the tonoplast (Supplemental Figure 2A). In the cell division zone, cell walls lying in between a pair of very narrow cells, which are likely newly formed daughter cells, were strongly labeled by GFP-KOR1 (Supplemental Figure 2B). This confirms an earlier observation by Zuo et al. (2000), reporting KOR1 localization at the cell plate of rapidly dividing tobacco (*Nicotiana tabacum*) BY-2 cells. Together with the observation that the GFP-KOR1 fusion used here fully reversed the *rsw2-1* growth phenotype, it appears that GFP-KOR1 regulated by its original promoter and terminator sequences is expressed in the correct tissues and targeted to its native location(s).

Defects in *N*-Glycosylation and the *rsw2-1* Mutation (G429R) Interfere with Efficient Targeting of GFP-KOR1 to the GA/TGN and the PM

We previously reported on a strong synergistic phenotype of *rsw2-1 stt3a-2* and *rsw2-1 cgl1-3* double mutant plants (Kang et al., 2008), indicating that attachment of *N*-glycans to KOR1 and their maturation may be essential for in vivo function. To dissect the impact of different *N*-glycosylation defects on KOR1 localization, the *GFP-KOR1* reporter construct was introduced into *cgl1-3* and *stt3a-2* plants, and the resulting subcellular distribution was analyzed (Figure 3). In *cgl1-3* host plants, the fluorescence pattern of GFP-KOR1 did not substantially differ from those in Col-0 or *rsw2-1*, showing extensive colocalization with the TGN marker (Figure 3A, panel d, white arrowheads) and adjacent location to the GA marker (Figure 3A, panel h, white arrowheads). This suggested that interfering with *N*-glycan maturation in the GA does not largely affect primary localization of GFP-KOR1, although PM labeling was occasionally missing (Supplemental Figure 2C). By contrast, substantial differences were observed when GFP-KOR1 was expressed in *stt3a-2* (Figure 3B). While GFP signals were

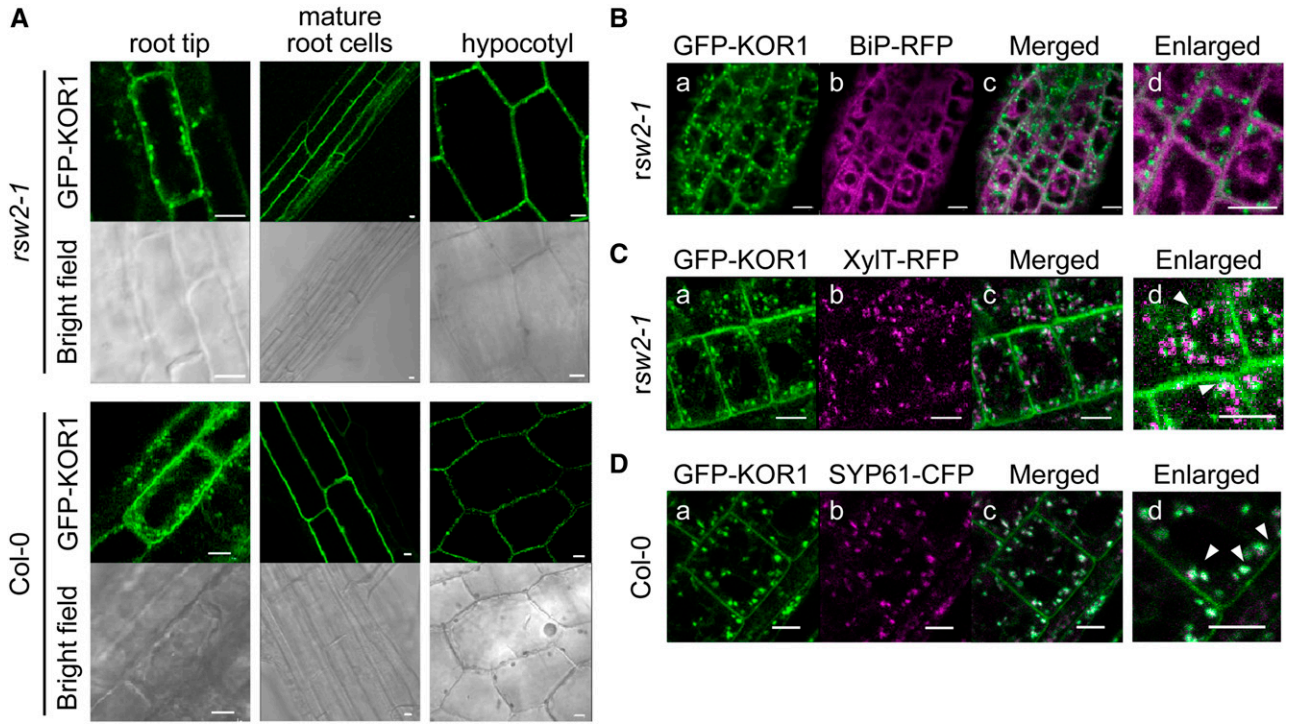

Figure 2. GFP-KOR1 Accumulates in the TGN and at the Plasma Membrane.

(A) Subcellular localization of GFP-KOR1 is not affected by the state of endogenous KOR1. Confocal images show GFP-KOR1 expressed in the *rsw2-1* mutant and in Col-0 wild type.

(B) to **(D)** GFP-KOR1 coexpressed with organelle markers labeling either the endoplasmic reticulum (BiP-RFP, **[B]**), the Golgi apparatus (XylT-RFP, **[C]**), or the TGN (SYP61-CFP, **[D]**). GFP channel (**[A]** to **[D]**, panel a), RFP channel (**[B]** and **[C]**, panel b), and CFP channel (**[D]**, panel b). Signals are merged in **(B)** to **(D)** (panels c and d). A part of the merged images was enlarged in (**[B]** to **[D]**, panel d). Arrowheads point to representative adjacent localization/colocalization of GFP and RFP/CFP (white signals) at the GA/TGN, respectively. Bars = 5 μm.

still observed in SYP61-positive TGN particles (Figure 3B, panel d, white arrowheads), an intracellular network of irregular shape was labeled as well. This was initially interpreted as ER, but the GFP-KOR1 pattern hardly overlapped with the ER marker BiP-RFP (Figure 3B, panel h). Instead, GFP-KOR1 signals often strongly labeled the periphery of vacuoles (Figure 3B, panels d and h, yellow arrowheads), indicative of GFP-KOR1 at the tonoplast. These data suggest that underglycosylation of KOR1 in the ER lumen increases mistargeting of KOR1 to tonoplasts in *stt3a-2*, although a biologically significant portion of GFP-KOR1 retained in the TGN likely suffices to exert its in vivo functions. This is consistent with the relatively normal phenotype of *stt3a* mutants grown under standard conditions. Together, these results suggest that attachment of *core N*-glycans (in the ER) is more important for proper targeting of KOR1 than maturation of complex *N*-glycans (in the GA).

Subcellular localization of GFP-RSW2-1 (obtained after introduction of the G429R mutation into KOR1) should be equivalent to KOR1 protein produced in *rsw2-1* host cells and was analyzed in the same way. Similar to the profile of wild-type GFP-KOR1 in *stt3a-2*, fluorescence signals of GFP-RSW2-1 in Col-0 were predominantly observed in the TGN (Figure 3C, panel d, white arrowheads) and at the tonoplast (Figure 3C, panels d and h, yellow arrowheads), but did not overlap with the ER marker BiP-RFP (Figure 3C, panel h). No clear signals were observed at the PM, suggesting that the G429R mutation in RSW2-1 promotes tonoplast targeting of the GFP-RSW2-1 protein, perhaps due to its instability/nonfunctionality. Moreover, this also showed that the presence of endogenous wild-type KOR1 protein does not rescue GFP-RSW2-1 localization via oligomerization. Although *rsw2-1* is a temperature-sensitive allele, growing plants at 18°C did not restore subcellular localization of GFP-RSW2-1 (data not shown). This is consistent with only partial growth recovery of *rsw2-1* mutant plants, even at the permissive temperature.

Systematic Mutagenesis of KOR1 *N*-Glycosylation Motifs Reveals Position-Specific Defects

Because KOR1 is underglycosylated in *stt3a* alleles, mislocalization of GFP-KOR1 in the *stt3a-2* background suggests that proper KOR1 targeting depends on the presence of its *N*-glycans. To determine if specific *N*-glycans important for targeting and function of KOR1 are missing in *stt3a*, we designed a series of KOR1 protein variants progressively decreasing in functional *N*-glycosylation sites, starting from less conserved peripheral sites to more conserved central sites (Δ-series) and finally those that contain only one intact *N*-glycosylation site (E-series). These GFP-KOR1 variants, flanked by native KOR1 promoter and terminator

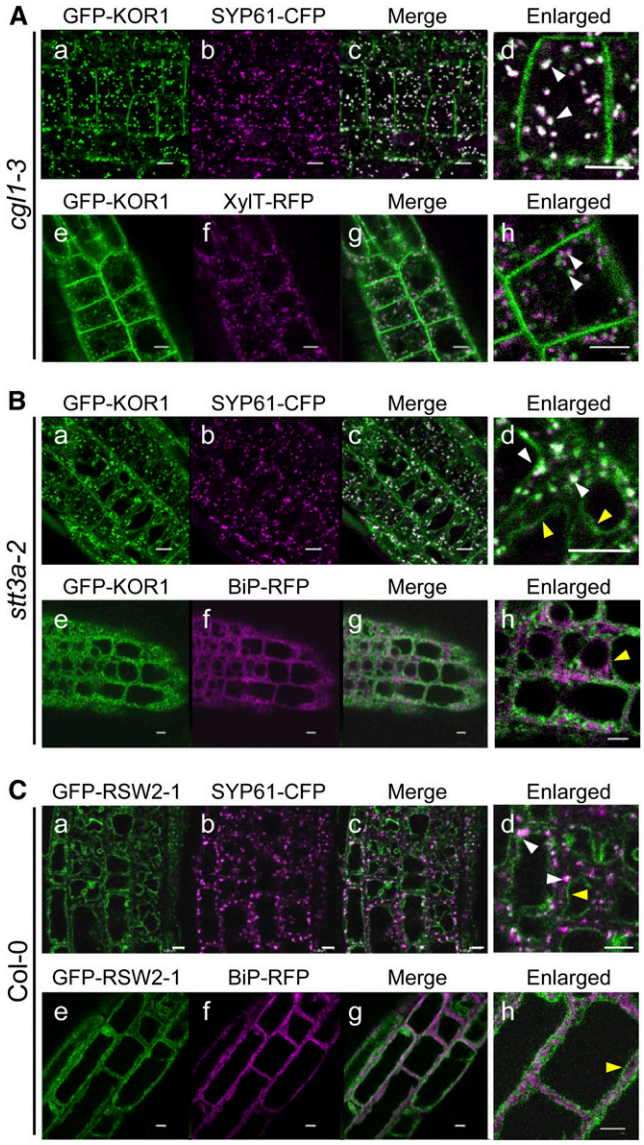

Figure 3. Impact of *N*-Glycosylation Defects and Mutations on Subcellular Localization of GFP-KOR1.

Host cell genotypes are: **(A)** *cgl1-3*, **(B)** *stt3a-2*, and **(C)** Col-0 wild type. GFP channel (a and e), CFP channel (b), and RFP channel (f). Signals are merged in (c, d, g, and h). A part of the merged images was enlarged (d and h). White arrowheads indicate adjacent localization/colocalization of GFP and RFP/CFP (white signals) at the GA/TGN, respectively. Yellow arrowheads indicate the tonoplast. Bars = 5 μm.

sequences, were expressed in the *rsw2-1* and in the *stt3a-2* background. Use of each *N*-glycosylation site in the transgenic lines was evaluated based on electrophoretic mobility of the denatured polypeptides by SDS-PAGE.

For this analysis, we first used the total insoluble fraction (including cell walls). Wild-type GFP-KOR1 migrated as a double band, consisting of a relatively sharp 110-kD and a fuzzy 100-kD band as detected by immunoblotting with anti-GFP antibodies (Supplemental Figure 3A). During the progressive loss of *N*-glycans, doublets were observed throughout, even for GFP-KOR1Δall without any *N*-glycan. The presence of the two forms cannot be due to cleavage of GFP-KOR1 because both the GFP domain close to the N terminus (amino acid position 31 to 272) and the N8 glycan (amino acid position 817) close to the C terminus (amino acid 871) were detected by anti-GFP antibodies (Supplemental Figure 3A, see mobility difference between Δ1 and Δ18). Cleavage of a short fragment at either the N or C terminus can also not explain the observed shifts. The possibility that the size differences are caused by *N*-glycan maturation is also unlikely because GFP-KOR1 without *N*-glycans (Δall, see below) shows doublet bands as well. Rather, doublet formation seems to be due to different folding states or abnormal binding of SDS to the transmembrane domain during sample preparation and electrophoresis (Rath et al., 2009). No major degradation product was visible for highly glycosylated GFP-KOR1, indicating that GFP fluorescence detected in the *rsw2-1* background largely represents intact GFP-KOR1. However, some smaller fragments (degradation products) were observed for GFP-KOR1 variants with only few, single, or no glycosylation (see E3 and Δall in Supplemental Figure 3A), indicating that multiple *N*-glycans are necessary to stabilize the protein.

Fractionation of total extracts using Miracloth filtration enriched for the low-mobility 110-kD form in the filtrate (Figure 4; Supplemental Figure 3B). Because the diffuse appearance of the high-mobility 100-kD bands rendered scoring of mobility shifts more difficult (particularly in the *stt3a-2* background), we hereafter used filtered extracts for immunoblot analysis and the low-mobility bands for our interpretations. As shown in Supplemental Figures 3A and 3B, the conclusions are the same. However, it should be noted that GFP-KOR1 in the filtrate is a minor fraction of total cellular

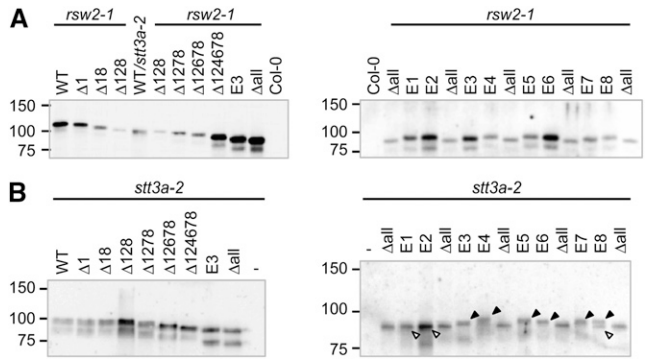

Figure 4. OST Complexes Use All the *N*-Glycosylation Sites of KOR1 in *rsw2-1*, but Not in the *stt3a*-2 Mutant.

Immunoblot analyses of *rsw2-1* **(A)** and *stt3a-2* **(B)** lines stably transformed with wild-type *GFP-KOR1* or Δ-series expression cassettes lacking *N*-glycosylation sites at the indicated positions or with E-series cassettes leaving a single *N*-glycosylation motif at the indicated position. Two-day-old seedlings were harvested. Pellet fractions of total protein extracts were separated in 6.25% SDS gels prior to blot development with anti-GFP antibodies (minus, untransformed *stt3a-2*). Electrophoresis was extended in the right blot of **(B)**. Filled arrowheads point to glycosylated and unfilled arrowheads to nonglycosylated E-series variants in the *stt3a-2* background. Col-0, wild type (untransformed). Size markers are given in kilodaltons.

GFP-KOR1 because ~20 times more protein (compared with samples containing cell walls) was needed for immunoblot analysis. Degraded GFP-KOR1 fragments were also enriched in the filtrate, which were not detectable in total cell extracts (Supplemental Figure 3A) and considered negligible.

As described above, in *rsw2-1* (complementation host), the GFP-KORΔ variants showed a stepwise increase in electrophoretic mobility with loss of each *N*-glycosylation site until all eight sites were removed, indicating that all N-X-S/T motifs in KOR1 are used (Figure 4A, left). This was confirmed by analyses of GFP-KOR1 E-series variants expressed in *rsw2-1*, all of which show slightly lower electrophoretic mobility compared with the GFP-KOR1Δall variant lacking all eight N-X-S/T motifs (Figure 4A, right). By contrast, the G429R mutation did not alter electrophoretic mobility of the intact GFP-RSW2-1 band, suggesting that RSW2-1 is properly *N*-glycosylated (Supplemental Figure 4). On the other hand, a general decrease in GFP-RSW2-1 protein and a higher level of fragmented GFP-RSW2-1 was observed, indicating instability of the RSW2-1 variant.

When expressed in *stt3a-2*, wild-type GFP-KOR1 showed similar mobility as GFP-KORΔ128 and Δ1278 variants expressed in *rsw2-1*, confirming underglycosylation of KOR1 (Figure 4A, left). Electrophoretic mobility of the GFP-KORΔ variants in *stt3a-2* did not change until 3 *N*-glycosylation sites were removed (Δ128; Figure 4B, left). This suggested that in the *stt3a-2* mutant, KOR1 receives only up to five *N*-glycans on average and lacks those close to both ends of the extracellular domain (N1, N2, and N8). Indeed, analyses of the GFP-KOR1 E-series variants expressed in *stt3a-2* revealed that E1 and E2 failed to receive a glycan (Figure 4B, right, unfilled arrowheads). On the other hand, the E8 variant showed a mixture of singly *N*-glycosylated and nonglycosylated polypeptides (Figure 4B, right, filled and unfilled arrowheads). These results established that the *stt3a-2* mutation particularly compromises *N*-glycosylation of less conserved sites close to the N and C termini of the luminal KOR1 domain.

Underglycosylated and Nonglycosylated KOR1 Partially Retain in Vivo Function

The GFP-KORΔ variants provided a unique opportunity to test whether the gradual loss of *N*-glycosylation on KOR1 correlates with reduced in planta function. For functional complementation tests, we used *rsw2-1* plants expressing *GFP-KOR1* cDNA constructs driven by the native regulatory sequences. To score for growth aberrations of the transformants (due to the large number of combinations handled), the first phenotypic survey was performed using segregating T2 plant material. Surprisingly, GFP-KORΔ variants missing up to six *N*-glycans were able to complement the root growth phenotype of *rsw2-1* to an extent similar to wild-type GFP-KOR1 (Figure 5). Plants transformed with the Δ2 construct exhibited slightly shorter roots compared with others, but this initial result did not reproduce in transformants with combined mutations (Δ12 to Δ125678). On the other hand, GFP-KOR1 lacking all eight *N*-glycans (Δall) showed only slight complementation in roots, confirming that decoration of KOR1 with at least one *N*-glycan is essential for normal root growth.

These results implied that each single *N*-glycan (by itself) might be sufficient for KOR1 function. To test this possibility, all GFP-KOR1 E-series variants were introduced into *rsw2-1* plants. The same survey protocol revealed much higher variability among the E-series transformants (Figure 5). Notably, GFP-KOR1 E1, E2, or E8 (containing only the 1st, 2nd, or 8th *N*-glycan) poorly complemented *rsw2-1* (Figure 5). This suggests that *N*-glycans at less conserved sites are not as effective in promoting KOR1 function as *N*-glycans at highly conserved sites. GFP-KOR1 E3 through E7 generally showed better complementation in this

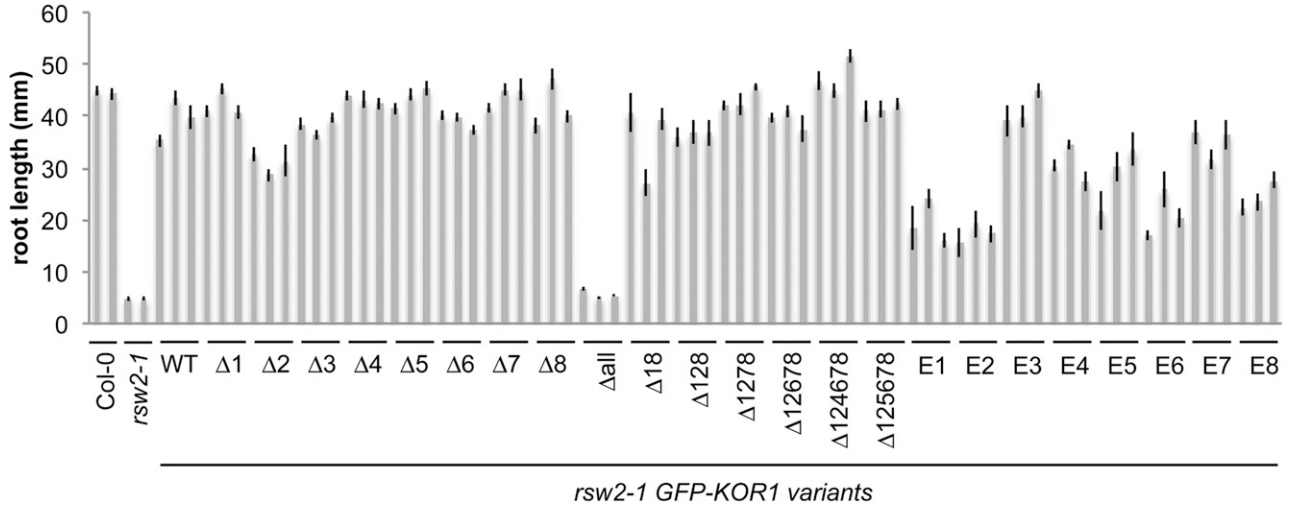

Figure 5. Effect of Differential *N*-Glycosylation on in Vivo Function of KOR1.

Growth of *rsw2-1* lines transformed with either *GFP-KOR1* wild-type, Δ-series, or E-series expression cassettes (driven by the original promoter and terminator sequences). Three independent T2 lines (n = 6 to 23 transformants per line) were analyzed for all listed constructs. Primary root length of 7-d-old seedlings was measured. Untransformed Col-0 wild type and *rsw2-1* plants served as control. Bars represent SE of the mean.

analysis, although variability was also observed among lines harboring the same transgene. Based on these observations, we hypothesized that (1) individual conserved *N*-glycans have different efficacies, (2) single *N*-glycan variants that are less effective produce barely sufficient levels of functional KOR1 to sustain normal root growth, and (3) variation among lines expressing the same KOR1 variant may be due to variability in individual transgene expression levels and/or subcellular targeting efficiency of the E variants.

To test these assumptions and to compare the efficacies of single *N*-glycans at the five highest conserved positions more reliably, additional complementation analyses were performed with genomic constructs. A wild-type *GFP-KOR1g* cassette and *GFP-KOR1gE3* through *gE7* variants thereof were prepared. Each variant contains the genomic coding sequence of KOR1 (including introns) so that the transgene structure is as close as possible to that of endogenous KOR1. Nonetheless, due to arbitrary integration, it is practically impossible to obtain transgenic lines that produce precisely the same level of GFP-KOR1 compared with endogenous KOR1. Therefore, a total of 10 transgenic lines were used to characterize each variant. As shown in Figure 6, expression of GFP-KORg (wild type), gE4, or gE7 in *rsw2-1* produced lines that grow similar to Col-0 with little line-to-line variability. The gE3 variant showed slightly higher line-to-line variability, and even greater variability was observed for the gE5 and gE6 variants, which scored the lowest average root growth. These results suggest that among the highly conserved central KOR1 *N*-glycans, positions N4 and N7 are the most effective and position N5 and N6 are the least effective ones.

Role of KOR1 *N*-Glycans in Protein Transport and Sorting

Underglycosylation and improper localization of GFP-KOR1 in *stt3a-2* suggested that *core N*-glycosylation is required for correct targeting of KOR1. Although *stt3a-2* mutant plants apparently skipped *N*-glycosylation of GFP-KOR1 only at less conserved positions N1, N2, and N8, a KOR1 variant lacking *N*-glycans at all three sites (Δ128) effectively complemented the *rsw2-1* mutant (Figure 5), demonstrating that *N*-glycans at these sites are not essential for KOR1 function. Consistently, GFP-KOR1 E1, E2, or E8 variants carrying a single *N*-glycan at peripheral positions (N1, N2, or N8), as well as GFP-KOR1Δall, did not effectively complement the *rsw2-1* mutation. Rather, a single *N*-glycan at any central site (between N3 and N7) conferred greater in vivo functionality to KOR1.

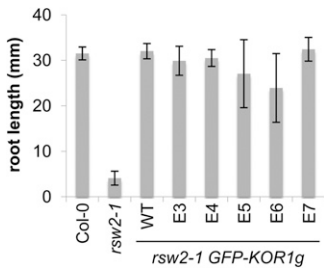

Figure 6. Effect of Single *N*-Glycosylation on in Vivo Function of KOR1.

Growth of *rsw2-1* lines stably transformed with *GFP-KOR1g* E-series expression cassettes (including introns). Ten independent T2 lines were analyzed per construct. Primary root length was recorded between day 4 and day 9 after germination. Untransformed Col-0 wild-type and *rsw2-1* plants served as control. Bars represent SD of 10 independent T2 lines (n = 16 to 34 transformants per line).

To determine the relationship between individual *N*-glycans and KOR1 targeting/function, subcellular localization of representative underglycosylated GFP-KOR1 variants was analyzed (Figure 7). GFP-KOR1Δ128, Δ12678 and GFP-KOR1 E3, E4, E5, E6, and E7 (containing at least one highly conserved *N*-glycan) showed a high degree of overlap with the TGN marker SYP61-CFP (Figures 7B, 7C, and 7E to 7I, panel d, white arrowheads). PM labeling was substantially decreased or lacking in the single *N*-glycan variants. Tonoplast staining increased in E3, E5, and E6 (Figures 7E, 7G, and 7H, panel d, yellow arrowheads), which showed less in vivo complementation activity than E4 or E7 in the root growth assay (Figure 6). By contrast, E1 and Δall plants displayed labeled tonoplasts (Figures 7D and 7J, panel d, yellow arrowheads). Similar to RSW2-1, some weak TGN signals were observed, even for these highly compromised KOR1 variants (Figures 7D and 7J, panel d, white arrowheads).

De Novo Expression of KOR1 in *Arabidopsis* Protoplasts

The above results suggested that KOR1 variants, either compromised by the G429R mutation or severe underglycosylation, are also targeted to tonoplasts. To determine if tonoplast membranes were the primary destination of such compromised KOR1 proteins, localization of selected GFP-KOR1 variants was analyzed upon transient expression in *Arabidopsis* protoplasts. Synchronized coexpression of GFP-KOR1 with selected marker constructs enabled us to determine the location where GFP-KOR1 variants initially accumulate. To test the capacity of mesophyll protoplasts to properly glycosylate GFP-KOR1 upon transient expression, we repeated the immunoblot analyses presented in Figure 4 using protoplast samples. As shown in Supplemental Figure 5, representative GFP-KOR1 variants produce *N*-glycosylation profiles similar to those obtained upon stable expression in transgenic plants. This suggests that short-term overexpression of GFP-KOR1 does not overload the *N*-glycosylation capacity of the cells. The predominant form of wild-type GFP-KOR1 produced in protoplasts was the low mobility form (110 kD), similar to GFP-KOR1 detected in the Miracloth filtrate of transgenic plant extracts. Generally, smaller bands were not observed in *rsw2-1* host cells during the course of the experiments. However, in *stt3a-2* host cells, an immunopositive band was visible below the 55-kD marker, indicative of some GFP-KOR1 degradation in *stt3a-2* (Supplemental Figure 5).

Subcellular localization of transiently expressed GFP-KOR1 was evaluated using a TGN marker (RFP-SYP61; Lam et al., 2009), an ER marker (OFP-ER; Frank et al., 2008), and a tonoplast marker (TPK1-RFP; Batistic, 2012) (Figure 8; Supplemental Figure 6). Wild-type GFP-KOR1 expressed in *rsw2-1* protoplasts initially gave rise to multiple particulate structures (Figure 8A; Supplemental Figure 6A). We found that intracellular particles were generally mobile and overlapped with the TGN marker (Figure 8A, panels c and f, white arrowheads). Small particles were also detected at the cell surface, but did not show mobility

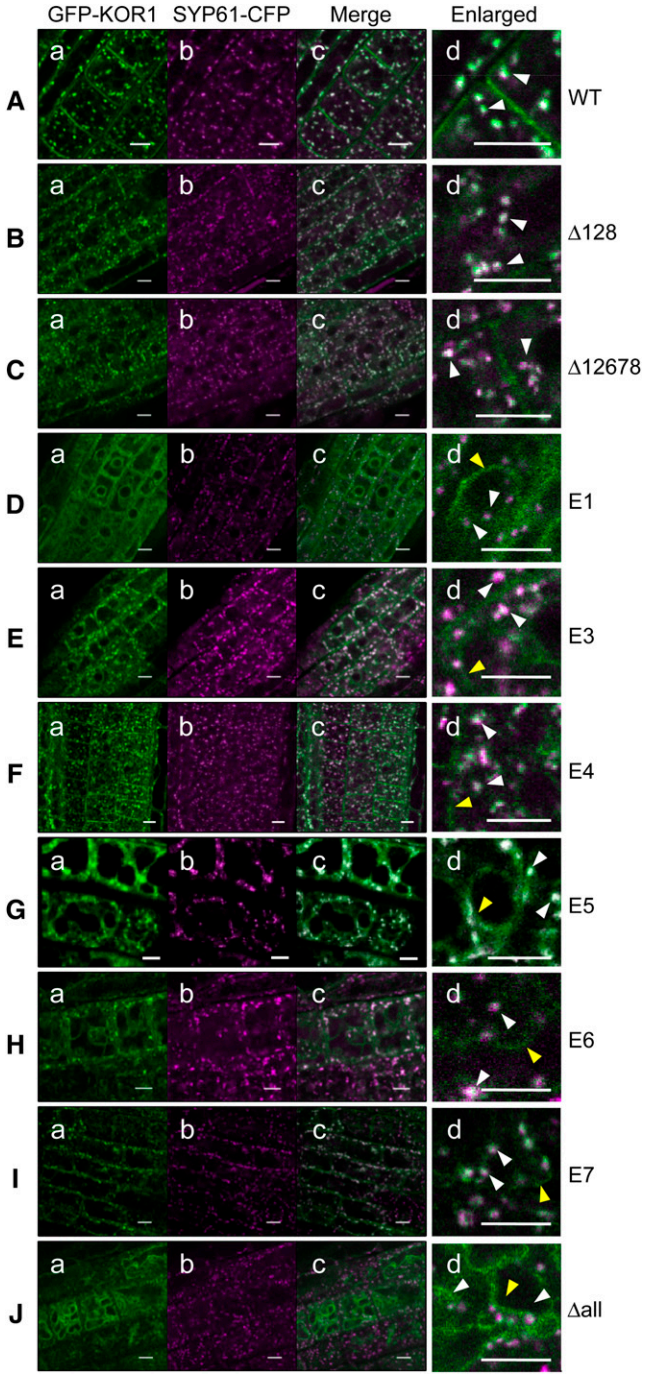

Figure 7. Localization of Wild-Type and Underglycosylated GFP-KOR1Δ- and E-Series Variants.

Confocal root cell images of 5-d-old transgenic seedlings coexpressing GFP-KOR1 and SYP61-CFP. Wild-type KOR1 **(A)** and underglycosylated GFP-KOR1 variants (**[B]** to **[J]**). GFP channel (a) and CFP channel (b). Signals are merged in panels c and d. A part of the merged images was enlarged (d). White arrowheads in enlarged images point to colocalization (white signals) at the TGN, yellow ones to tonoplast rims. Bars = 5 μm.

(Figure 8A, panels c and f, red arrowheads). These particles likely represent GFP-KOR1 delivered to the PM. Later (at 48 h after transfection), GFP-KOR1 signals increased at the PM, appearing as bright particles and patches and weakly diffuse signals on the cell surface (Figure 8A, panels i and l, red arrowheads). GFP-KOR1 expressed in *stt3a-2* protoplasts, as well as GFP-RSW2-1 in *rsw2-1*, similarly produced mobile intracellular TGN particles and spots on the cell surface at 24 h after transfection (Figures 8B, and 8C, panels c and f, white arrowheads). However, at 48 h after transfection, GFP-RSW2-1 in *rsw2-1* and GFP-KOR1 in *stt3a-2* (to a lesser extent) developed tonoplast-localized GFP signals (Figures 8B and 8C, panels g, i, j, and l, yellow arrowheads). *stt3a-2* cells produced surface patches similar to *rsw2-1* cells (compared with Figures 8A and 8B, panels j and l, red arrowheads), but GFP-RSW2-1 produced only weak and smaller dots on the cell surface (Figure 8C, panels c, f, j, and l, red arrowheads). This indicates that RSW2-1 reaches the TGN, but instead of being effectively delivered to the PM, it is directed to tonoplasts.

In stark contrast, GFP signals produced by GFP-KOR1Δall predominantly overlapped with the OFP-ER marker, both at 24 and 48 h after transfection (Figure 8D; Supplemental Figure 6D, panels c, f, i, and l). Nevertheless, a small fraction of GFP-KOR1Δall exited the ER because in some cells GFP signals overlapped with TGN particles labeled by RFP-SYP61 at 24 h after transfection (Supplemental Figure 7A, panels c, f, and i, white arrowheads). At 48 h after transfection, GFP signals were also observed in structures that did not overlap with the ER marker (Figure 8D, panel i, green areas). Coexpression of GFP-KOR1Δall with the tonoplast marker (TPK1-RFP) revealed weak tonoplast labeling of GFP-KOR1Δall at 48 h (Supplemental Figure 7B, panels c, f, and i, yellow arrowheads). Similar to other transfected protoplasts, nonmobile GFP-positive particles were detected in some, but not all, GFP-KOR1Δall cells (Supplemental Figures 7A and 7B, panel l, red arrowheads). Apparently, the majority of newly synthesized GFP-KOR1Δall is trapped in the ER, and only a small share of GFP-KOR1Δall proteins reaches the TGN, where they are targeted to the PM or tonoplasts.

These results demonstrate that the G429R mutation in RSW2-1, KOR1 underglycosylation in *stt3a-2* host cells, and no glycosylation of KOR1Δall have distinct impacts on de novo-synthesized GFP-KOR1. The *stt3a-2* host mutation was the least severe of all three genetic perturbations, consistent with normal growth of *stt3a-2* plants under standard conditions. Unlike GFP-KOR1Δall, GFP-RSW2-1 did not accumulate in the ER, suggesting successful folding. However, rapid accumulation of GFP-RSW2-1 in tonoplast membranes and protein fragmentation is indicative of its enhanced cellular turnover.

Physical Presence of Complex *N*-Glycans on KOR1

The above results demonstrated that *N*-glycans at positions N3, N4, and N7 sufficiently promote proper folding and TGN/PM delivery to support in vivo function of KOR1. Our previous genetic analyses suggested that maturation of *N*-glycans in the GA is important for KOR1 function (Kang et al., 2008), but questions remained about whether specific modifications are required and which position needed modification. Furthermore, the actual presence

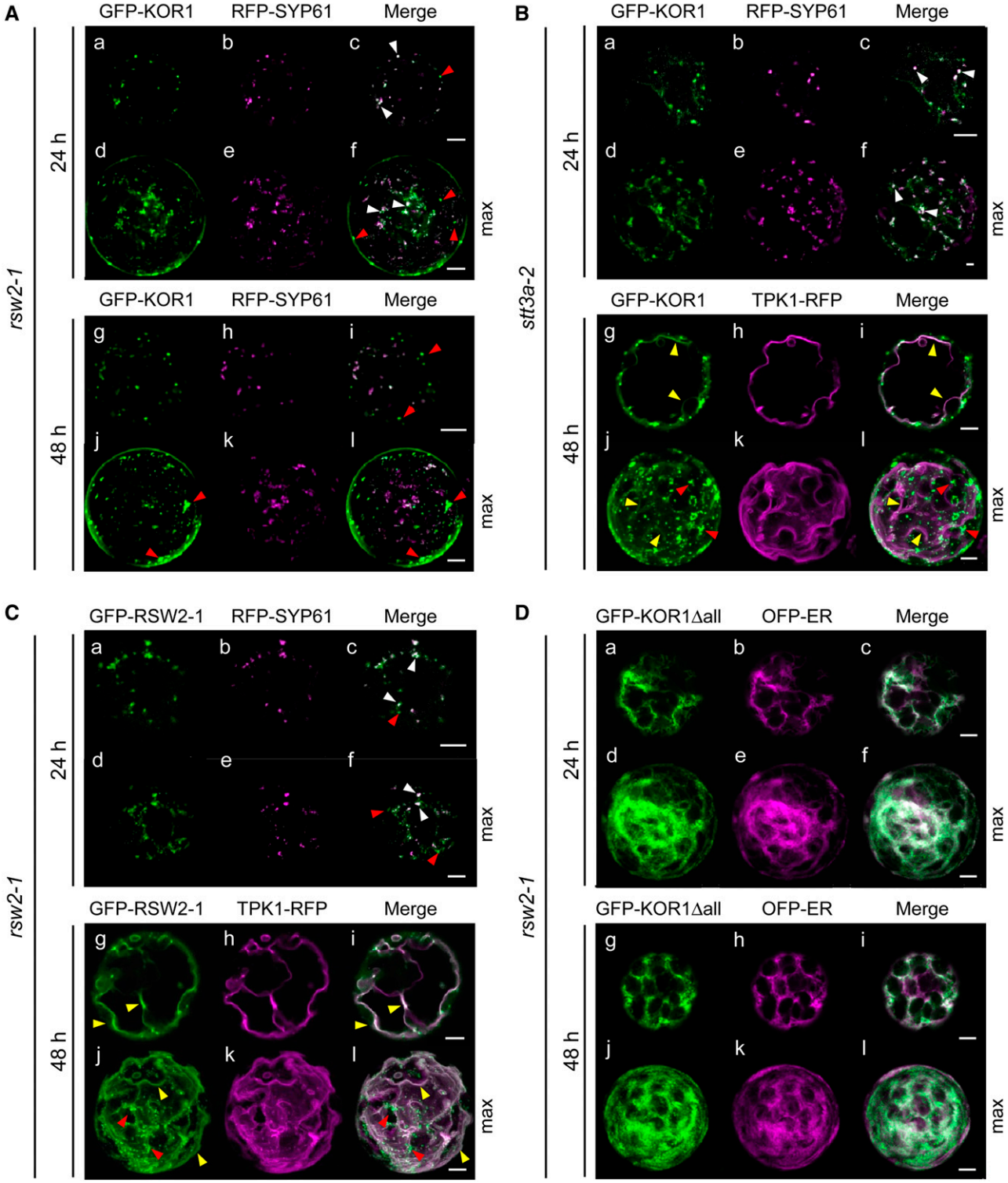

Figure 8. Transition of Subcellular Localization of GFP-KOR1 Variants Synthesized de Novo in *Arabidopsis* Protoplasts.

GFP-KOR1 expressed in *rsw2-1* **(A)** or *stt3a-2* protoplasts **(B)**, GFP-RSW2-1 in *rsw2-1* **(C)**, and GFP-KOR1Δall in *rsw2-1* **(D)** was documented by confocal microscopy. Signals corresponding to the TGN or tonoplasts were identified by coexpressing RFP-SYP61 or TPK1-RFP, respectively (24 and 48 h after transfection). GFP channel (a, d, g, and j), RFP channel (**[A]** to **[C]**, b, e, h, and k), and orange fluorescent protein (OFP) channel (**[D],** b, e, h, and k). Signals are merged in panels c, f, i, and l. Lower panels are maximum projections (max) of ~30 sections from the same cell (one shown in upper panels). White arrowheads point to colocalization (white signals) at the TGN, yellow ones to tonoplast rims, and red ones to GFP-KOR1 patches at the cell surface. Bars = 5 μm.

of complex *N*-glycans attached to KOR1 had not been assessed directly in *Arabidopsis*. To clarify these issues, 6xHis-tagged KOR1 (RGS-His-KOR1) stably expressed in *Arabidopsis irx2-1* (*kor1* allele) (Szyjanowicz et al., 2004) was affinity-purified using Ni^{2+}-NTA Sepharose chromatography. Because the RGS-His-KOR1 fraction that eluted from the Ni^{2+}-NTA column still contained substantial contaminating material, aliquots were resolved by 2D-PAGE. As shown in Supplemental Figure 8, immunoblotting with complex glycan-specific antibodies (α-cgly) visualized a predominant, vertically elongated signal that corresponds to the one visualized by RGS-His antibodies (α-RGS-His). This revealed that KOR1 polypeptides are indeed decorated with complex *N*-glycans. As observed earlier with GFP-KOR1 (Supplemental Figure 3), also RGS-His-KOR1 showed anomalous electrophoretic mobility. Therefore, vertical elongation of the KOR1 spot unlikely represents heterogeneity in site occupancy of *N*-glycans, but rather denaturation intermediates and/or detergent binding states during 2D-PAGE that uses urea and different detergents (Rath et al., 2009). Modification of the majority of KOR1 *N*-glycans to complex types was further supported by conventional SDS-PAGE/immunoblot analysis of transgenic plants stably expressing GFP-KOR1. *N*-glycans of GFP-KOR1 in Col-0 wild type, but not in the *cgl1-3* mutant, were highly resistant to diagnostic PNGase-F treatment (Supplemental Figure 9, arrow), indicating that KOR1 in the wild type is mostly decorated with complex *N*-glycans carrying *core* α1,3-fucose modification.

Complex *N*-Glycans May Promote KOR1 Function in *Trans*

The requirement for specific *N*-glycan modifications to grant KOR1 function was assessed genetically (Kang et al., 2008). *rsw2-1* plants were crossed with several mutants that are defective in selected glycosidase or glycosyltransferase activities in the Golgi apparatus. The resulting double to quadruple mutants were evaluated for synergistic effects of complex *N*-glycosylation defects and the *rsw2-1* mutation. As depicted in Figure 9, *rsw2-1 hgl1-1* plants, additionally lacking Golgi α-mannosidase II, showed similar root growth defects at 18°C (permissive temperature) as previously described for *rsw2-1 cgl1-3* plants, additionally lacking GnTI (Kang et al., 2008). Importantly, mutation of GnTII, preventing GlcNac modification of the α1,6-mannose arm, or β1,3-galactosyltransferase (GalT), lacking ability to form Lewis a epitopes (Strasser et al., 2007b) (Figure 9B), did not enhance the *rsw2-1* root phenotype. Growth of *rsw2-1 xylT* was similar to *rsw2-1*, whereas loss of *core* fucosylation in *rsw2-1 fucTa fucTb* (*fucTa/b*) enhanced the root growth defect of the *rsw2-1* mutant. In accordance with the negligible effect of *xylT*, additional root growth inhibition of *rsw2-1 xylT fucTa/b* mutant plants was small. These results reveal that *core* α1,3-fucose attachment is an important host *N*-glycan modification for in vivo functionality of KOR1. However, this is not more important than mannose trimming (Figure 9B) because persisting mannoses on the α1,6-branch produce more severely impaired phenotypes in *rsw2-1 hgl1-1* whose *N*-glycans still receive *core* α1,3-fucose (Strasser et al., 2006; Kaulfürst-Soboll et al., 2011). Neither *hgl1-1* nor *fucTa/b* double mutants without *rsw2-1* showed growth defects in the absence of osmotic stress (Kang et al., 2008).

The above results, as well as our previous reports (Frank et al., 2008; Kang et al., 2008; von Schaewen et al., 2008), indicate that

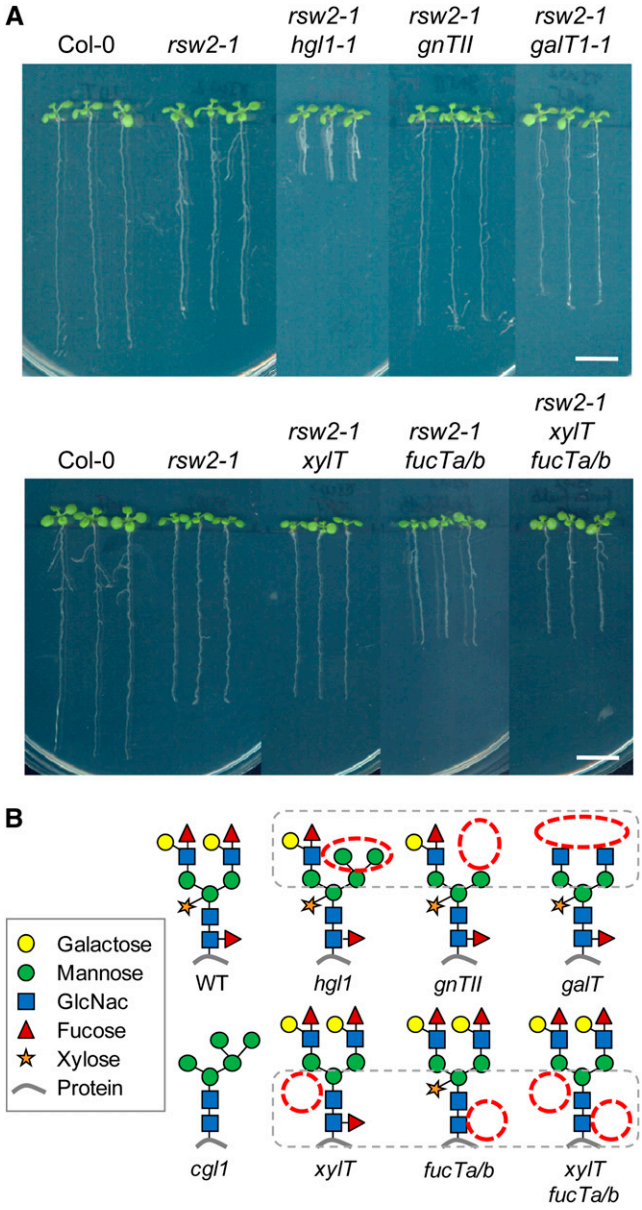

Figure 9. Genetic Interaction between *rsw2-1* and Mutations Affecting Complex *N*-Glycan Maturation in the Golgi Apparatus.

(A) Only *hgl1* and *fucTa/b*, but no other mutations of the complex *N*-glycan maturation pathway, enhance the root growth phenotype of *rsw2-1*. Plants were grown on quarter-strength MS salts and 0.5% sucrose for 11 d at 18°C and photographed. Bars = 5 mm.

(B) Scheme of *N*-glycan maturation defects of the mutant lines used in this study. Red circles/ovals highlight residues that either persist or are missing (top, antenna maturation; bottom, *core* *N*-glycan modification).

formation of mature complex *N*-glycans grants in vivo root growth. To test if this occurs in *cis*, i.e., via direct influence of *N*-glycans attached to the KOR1 polypeptide, we tested the impact of abrogating complex *N*-glycan modification by the *cgl1-3* mutation on *rsw2-1* expressing GFP-KOR1Δall (Figure 10). To minimize variation due to transgene integration, we first introduced the

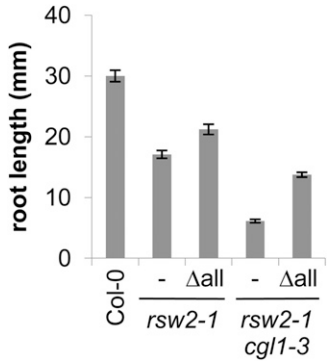

Figure 10. Genetic Interaction between GFP-KOR1Δall and *cgl1-3*.

Plants were germinated on agar medium containing quarter-strength MS salts and 0.5% sucrose for 5 d at 18°C and then grown for an additional 6 d at 25°C. The data show mean values (n = 28 to 34 plants per genotype) of primary root length at 25°C. Experiments were repeated twice with similar results. Δall, plants transformed with *GFP-KOR1Δall*; −, untransformed plants. Bars represent SE of the mean.

GFP-KOR1Δall construct into the *rsw2-1 cgl1-3* double mutant. Then, a homozygous T3 line was crossed with the *rsw2-1* mutant to obtain F1 seeds with [*rsw2-1 CGL1/cgl1-3 GFP-KOR1Δall/-*] genotype, which we refer to as *rsw2-1 GFP-KOR1Δall*. When using agar medium containing quarter-strength Murashige and Skoog (MS) salts and 0.5% sucrose, root growth of *rsw2-1 GFP-KOR1Δall* exceeded that of *rsw2-1* (Figure 10, minus sign) indicating that the GFP-KOR1Δall variant partially retains KOR1 function, independent of *N*-glycan attachment. Similarly, *rsw2-1 cgl1-3* was partially complemented by *GFP-KOR1Δall*. When all four genotypes are compared, it becomes evident that *cgl1-3* (no complex *N*-glycans) reduces growth of both parental *rsw2-1* mutant lines and also of *rsw2-1* complemented by *GFP-KOR1Δall* (Figure 10, compare minus to Δall). This indicates that *cgl1-3* still affects the function of nonglycosylated KOR1. Thus, complex *N*-glycans (not attached to KOR1) seem to promote KOR1 function in *trans*, suggesting that accessory factors with complex *N*-glycans contribute to KOR1 function and/or additional mechanisms cooperate with KOR1 during cell wall biosynthesis.

DISCUSSION

Here, we report the systematic characterization of the role of *N*-glycosylation in KOR1 function. The *Arabidopsis* proteome comprises ~4000 secreted/membrane proteins (excluding mitochondrial and chloroplast proteins) with at least one *N*-glycosylation site, and of these, ~1200 proteins contain more than five potential *N*-glycosylation sites. To date, only limited information is available concerning the role of individual *N*-glycans on such glycoproteins. In *Arabidopsis*, the role of *N*-glycans has been studied in most detail with elongation factor Tu (EF-Tu) receptor (EFR) in the innate immunity pathway, pointing to a single essential *N*-glycan at position N143 for receptor-ligand interaction (Häweker et al., 2010). Interestingly, EFR function was not affected by defects in Golgi-resident *N*-glycan modification enzymes, indicating that the presence of any *N*-glycan type at N143 is sufficient for innate immunity signaling. Our data obtained with KOR1 reveal a more complex nature of *N*-glycans for an extracellular catalytic domain. First, among a total of eight *N*-glycans attached to KOR1, no single *N*-glycan was essential for KOR1 function. However, multiple *N*-glycans were needed for stable accumulation of KOR1 in proper subcellular compartments (TGN/PM), and at least one *N*-glycan on KOR1 was required for efficient exit from the ER. Second, a single *N*-glycan attached at a less conserved site (N1, N2, or N8) was the least functional. Because N1/N2 locate toward the transmembrane region of the protein and N8 resides close to the C terminus, isolated single *N*-glycosylation of these positions may not effectively recruit lectin chaperones during protein folding in the ER and/or fails to stabilize KOR1 after folding. Even among the highly conserved sites, single *N*-glycosylation of N3, N4, or N7 offered better functionality than of N5 or N6.

The KOR1 localization results obtained in this study integrate previous observations made with various experimental systems (Nicol et al., 1998; Zuo et al., 2000; Robert et al., 2005; Drakakaki et al., 2012). Furthermore, the subcellular patterns obtained in the stable transgenic lines and in the transient protoplast expression system revealed multiple regulatory checkpoints that determine the fate of GFP-KOR1 in the secretory pathway. As depicted in Figure 11, newly synthesized GFP-KOR1 is subject to chaperon-aided protein folding in the ER during quality control cycles (ERQC). A great proportion of nonglycosylated GFP-KOR1Δall that does not fold properly is retained in the ER lumen and likely destroyed via ER-associated protein degradation (Vembar and Brodsky, 2008). Once exported from the ER, all GFP-KOR1 variants analyzed in stably transformed lines showed some level of accumulation at the TGN. This was especially obvious for de novo-synthesized wild-type GFP-KOR1 and its variants in freshly transfected protoplasts, suggesting that GFP-KOR1 variants leaving the ER are initially delivered to the TGN. At the TGN, *N*-glycans seem to have a major impact on the fate of KOR1: The protein is first retained in the TGN and then sorted to the PM. The nature of the *trans* effect of complex *N*-glycans has yet to be determined, but likely affects post-Golgi processes, such as stabilization and distribution of KOR1 within the TGN and PM, either directly or indirectly. On the other hand, severely underglycosylated/nonglycosylated GFP-KOR1 variants were neither effectively retained in the TGN nor targeted to the PM. Unless one or more *N*-glycans were present at conserved sites, GFP-KOR1 variants accumulated at the periphery of vacuoles. Such tonoplastic accumulation was observed also with GFP-RSW2-1, whose temperature-sensitive property likely causes folding instability/dysfunctionality of the luminal domain. Because *N*-glycan attachment to proteins often increases their stability (Skropeta, 2009), it appears that tonoplast sorting of GFP-KOR1 at the TGN is determined by the stability and folding state of the protein. This could be similar to the way that cells dispose of damaged KOR1 during natural protein turnover. Consistently, very weak tonoplast labeling was observed even with transgenic plants expressing intact, wild-type GFP-KOR1 (Supplemental Figure 2A). Based on the functional connection of KOR1 and the cellulose synthase complex (CSC) at the PM, as well as their colocalization at the TGN (Drakakaki et al., 2012), KOR1 may be retrieved by endocytosis similar to the CSCs (Bashline et al., 2013) or together with them. A recent report on another root swelling mutant, *rsw9*,

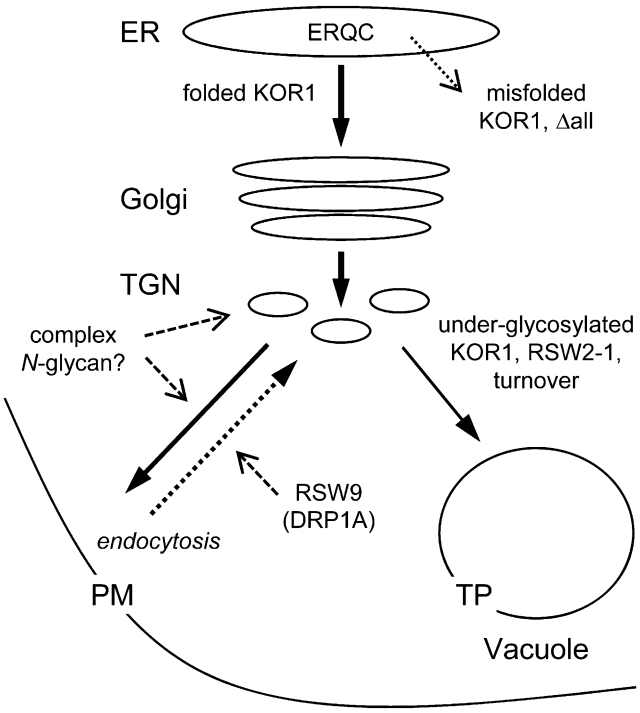

Figure 11. Scheme Depicting the Fate of Wild-Type, Underglycosylated, or Mutated KOR1 in *Arabidopsis* Cells.

Wild-type KOR1 receives eight *N*-glycans in the ER that are modified to complex types in the GA (Golgi) and localize in the TGN prior to delivery to the PM. The PM localization is not dependent on (but may be affected by) the state of complex *N*-glycan maturation of yet unknown factors (?). Total lack of *N*-glycosylation on KOR1Δall results in ERQC and partial degradation in the cytosol. Underglycosylated KOR1 or dysfunctional RSW2-1 (G429R; Figure 1A) that reach the TGN are not efficiently delivered to the PM. Instead, these KOR1 variants are directed to the tonoplast (TP). The latter likely also represents the native turnover pathway for aged/damaged, endogenous KOR1 upon endocytosis, possibly via RSW9, encoding dynamin-related protein 1A (DRP1A).

supports this hypothesis. *RSW9* encodes a dynamin-like (motor) protein important for endocytosis, and the *rsw9* mutation causes a cellulose deficiency phenotype similar to *rsw2-1* and other cellulose biosynthesis mutants (Collings et al., 2008).

Dissection of the *N*-glycosylation pattern of GFP-KOR1 in the *stt3a-2* mutant revealed position specificity of the OST complex that harbors exclusively STT3B (Koiwa et al., 2003). In mammalian cells, OST complexes containing STT3A (which is similar to *Arabidopsis* STT3B) conduct cotranslational *N*-glycosylation, whereas complexes harboring STT3B (similar to *Arabidopsis* STT3A) may function posttranslationally (Ruiz-Canada et al., 2009). Their analyses showed that *N*-glycosylation sites close to transmembrane regions or to the C termini of polypeptides were not efficiently used by OST complexes containing human STT3A (equivalent to *Arabidopsis* STT3B). Because N1 and N2 sites are located relatively close to the transmembrane region of KOR1, lack of *N*-glycan addition to E1 and E2 variants in *stt3a-2* is consistent with the expected specificity of STT3 isoforms as inferred from the corresponding human OST complexes (Ruiz-Canada et al., 2009). Moreover, this can also explain lack of N1 and N2 glycosylation and incomplete N8 glycosylation observed in *stt3a-2*. However, these are not sufficient to account for the reduction in molecular mass of GFP-KOR1 in *stt3a-2* (Figure 4A). In addition, the subcellular localization profile of GFP-KOR1 in *stt3a-2* resembles more that of GFP-KOR1 variants lacking six to eight *N*-glycans than that of GFP-KOR1Δ128. Together, this suggests that global underglycosylation and activation of the unfolded protein response in *stt3a-2* (Koiwa et al., 2003; Kang et al., 2008) additionally compromise even mildly underglycosylated GFP-KOR1, which results in enhanced targeting to tonoplasts. Notably, the polarized targeting signal identified in the cytosolic domain of KOR1 by Zuo et al. (2000) contains a di-leucine motif at position 48-49 that is part of a tonoplast targeting motif [D/E] $X_{3\text{-}5}$L[L/I] identified in plant intrinsic membrane proteins (Pedrazzini et al., 2013). Perhaps the status of KOR1, i.e., folding and association with CSCs (Vain et al., 2014) as well as the developmental stage of cells, affects the context of targeting between the PM and tonoplasts, which is decided in the TGN.

N-glycans can determine the function of mature glycoproteins by mechanisms including improvement of thermal stability and/or catalytic activity (Adney et al., 2009; Voutilainen et al., 2010; Kayser et al., 2011). The structural study of glycoside hydrolase 9-family proteins provided some insights into the role of *N*-glycans on KOR1 after folding. Compared with the highly active prokaryotic homolog TfCel9A (*Thermobifida fusca* Cel9A), KOR1 family proteins from plants exhibit substitutions in their substrate binding sites. These substitutions replace multiple Trp residues in binding sites for -4, -3, and -2 glucose units, which stabilize enzyme-substrate interactions. Consequently, in one study, the relative activity of PttCel9A (*Populus tremula* × *tremuloides* KOR1 homolog) was 0.04% of TfCel9A (Master et al., 2004). One of the substitutions (Ser-326 in KOR1 replaces Trp in the -3 position) creates an *N*-glycosylation site that is conserved in all plant isoforms (N4). The presence of an *N*-glycan structure close to the active site cleft can potentially hinder enzyme function similar to the blocking loop present in TfCel9A (359-369 in KOR1/PttCel9A). However, for the plant KOR1 homologs, a beneficial effect has been proposed based on high conservation of the loop sequences (Master et al., 2004). Here, we show that single *N*-glycan decoration at position N4 (E4 variant), as well as N7 that resides on the other side of the active site cleft, have the most positive in vivo effect of the eight KOR1 *N*-glycans. Because recombinant PttCel9A produced in *Pichia pastoris* lost up to 80% of its activity upon deglycosylation, it is conceivable that some *N*-glycans on KOR1, such as N4 and N7, act synergistically with the blocking loop (shaded gray in the 3D model, Figure 1B) in aligning the fibrous substrate along the active site cleft.

But what is the effect of compromised complex *N*-glycan maturation on KOR1? As revealed here, even plants expressing nonglycosylated KOR1 are negatively impacted by the *cgl1* mutation. This suggests that defects in *N*-glycan maturation in the GA compromise multiple factors of cell wall assembly simultaneously, albeit without decreasing wall-forming capacity below the threshold level because such a reduction would only become visible in synergy with the *rsw2-1* mutation or when challenged by osmotic stress (Kang et al., 2008). Candidates for such factors include COBRA, a glycosylphosphatidylinositol-anchored

cell surface protein also involved in cellulose biosynthesis, because genetically blocking *N*-glycan maturation at the step of mannose trimming in the ER enhanced root swelling of the *cob* mutant (Roudier et al., 2005; Liebminger et al., 2009). Another possibility is that the presence of glycoprotein factors with complex *N*-glycan decorations function in *trans* to promote proper post-TGN trafficking/function of KOR1 and related proteins because we observed that GFP-KOR1 in the *cgl1* host, as well as underglycosylated GFP-KOR1, occasionally failed to accumulate at the PM. Proper delivery/recruitment of KOR1 to/from the PM/TGN may be regulated by glycoproteins with complex *N*-glycans or proteins that recognize/bind to certain complex *N*-glycan epitopes, e.g., the mature (trimmed) α1,6-branch and/or *core* α1,3-fucose. Stronger effects caused by *cgl1* or *hgl1* could be attributed to persisting mannoses on the α1,6-branch, but in the case of *hgl1*, also alter the availability/accessibility of *core* fucoses. We previously demonstrated that the α1,3-fucose epitope present in *hgl1* mutants was recognized by complex glycan- and fucose-specific antibodies only after enzymatic digestion of the bulky mannoses on the α1,6-arm (Kaulfürst-Soboll et al., 2011). These immunologic and modeling results support our hypothesis that complex *N*-glycans could function as an important interface between glycoproteins and their interacting partners. Indeed, at least 46 proteins encoding receptor-like kinases with extracellular lectin binding domains are present in the *Arabidopsis* genome (Barre et al., 2002), some of which are involved in cellulose biosynthesis (Hématy et al., 2007; Xu et al., 2008). Considering the close connection between cellulose biosynthesis, KOR1 trafficking, and microtubule organization (Lei et al., 2014), it is also possible that glycoprotein adaptors somehow facilitate engagement of KOR1 with microtubules on the cytoplasmic face of the membrane. Clearly, these possibilities are not mutually exclusive and perhaps occur in parallel. Interestingly, some F-box proteins containing a lectin-like domain can bind to various carbohydrate epitopes including *core* α1,3-fucose, implying a role for complex *N*-glycans in protein turnover (Stefanowicz et al., 2012). In addition, a recent report showed that KOR1 is part of the cellulose synthase complex required for normal motility and intracellular trafficking of the CSC (Vain et al., 2014). Therefore, functional interplay between complex *N*-glycans and KOR1 in the TGN emerges as an input point that regulates cellulose biosynthesis according to growth and environmental signals.

METHODS

Plant Materials

The *Arabidopsis thaliana* Col-0 ecotype was used throughout this study. Mutant lines *stt3a-2*, *cgl1-3 rsw2-1*, *hgl1-2*, *fucTa fucTb* (*fucTa/b*), and *xylT* were described previously (Kang et al., 2008); seed stock of the *galT1-1* (SAIL_170_A08) line was provided by Kyun Oh Lee (Gyeongsang National University), and *gnTII* (FLAG_394A11) was from the Institut National de la Recherche Agronomique, Versailles (Samson et al., 2002).

Bioinformatic Analysis

To calculate *N*-glycosylation site conservation, sequences of KOR1 homologs were first identified by searching plant protein data sets using BLASTP. Fifty-two nonredundant sequences from 22 species were identified. Multiple sequence alignments were performed using NCBI COBALT.

Construction of KOR1 3D Model

A 3D model of KOR1 (At5g49720) was obtained by SWISS-MODEL, an automated comparative protein modeling server at http://swissmodel.expasy.org/workspace (Guex and Peitsch, 1997; Schwede et al., 2003; Arnold et al., 2006), using an insect endoglucanase as template [1KS8A] (1.40 Å). The resulting PDB file was uploaded to GlyProt, enabling attachment of selected *N*-glycans to the protein backbone via SWEET2 at http://www.glycosciences.de/modeling/glyprot/, a service of the German Cancer Research Centre (DKFZ Heidelberg). The new PDB file was further modified with Jmol, an open-source Java viewer for chemical structures in 3D (http://www.jmol.org/).

Plant Growth Assays

For routine in vitro culture, surface-sterilized seeds were sown on media containing quarter-strength MS salts, 0.5% sucrose, and 1.5% agar. After stratification for 2 to 4 d at 4°C, plates were incubated in vertical position at 23°C for 7 d under a 16-h-light/8-h-dark cycle.

For root growth analyses, seeds were sown on medium containing 1× MS salts, 3% sucrose, and 1.5% agar and processed as above. After 5 d at 23°C, the positions of root tips were marked and plants were kept under the same culture condition for five more days before taking photographs. Root growth between days 5 and 10 was determined using ImageJ software. For analysis of GFP-Kor1Δall, seeds were sown on medium containing quarter-strength MS salts, 0.5% sucrose, and 1.5% agar. The root tip positions were marked after incubation for 4 d at 18°C, and plates were incubated for six additional days at 25°C before documentation and data analysis.

Construction of GFP-KOR1 Expression Cassettes

Primer sequences used in this study are listed in Supplemental Table 1. A pCAMBIA plasmid with the RGS-His-modified genomic KOR1 fragment (RGS-His-KOR1) was obtained from Simon Turner (University of Manchester, UK). The RGS-His-KOR1 fragment (corresponding to position 20202219 to 20197148 on chromosome 5) was excised with *Sal*I/*Eco*RI and cloned into similarly digested pENTR2B to produce pEnKORg. A silent mutation (T to G) was introduced at position 20199877 to create a *Sac*II restriction site. To produce pEnKORc, a *KOR1*-cDNA fragment was amplified using primer pair [765, 997] and cloned into the *Sac*II/*Bst*XI sites of pEnKORg. To create pEnGFPKORc and pEnGUSKORc, GFP- and GUS-coding sequences lacking stop codons were amplified using primer pairs [1063, 1064] and [1065, 1066], respectively, digested by *Bgl*II, and inserted at the unique *Bam*HI site inside the RGS-His tag within the cytoplasmic domain of pEnKORc. For transient expression in protoplasts, pEnSOGFP-KOR1, in which the KOR1 promoter was replaced by a synthetic constitutive promoter (Ni et al., 1995), was prepared.

Mutations at KOR1 *N*-glycosylation motifs and the G429R mutation were introduced as described previously (Frank et al., 2008) using the QuickChange site-directed mutagenesis kit protocol (Stratagene) and Phusion DNA Polymerase (Finnzymes/Thermo-Scientific). As mutagenesis template, pGFP2ΔNco-KOR1 was prepared by inserting the KOR1cDNA fragment amplified with primers [KOR-XbaI-s, KOR-XhoI-as] and inserted via *Xba*I/*Xho*I into pGFP2ΔNco. Primers used in the mutagenesis are listed in Supplemental Table 1. Mutated fragments were confirmed by sequencing (Seqlab), amplified by primer pair [765, 997], and cloned via *Sac*II/*Bst*XI into pEnGFPKORc for complementation and pEnSOGFPKORc for transient expression analyses.

Organelle Markers

BiP-RFP and XylT-RFP were prepared using recombineering procedures (Rozwadowski et al., 2008). BAC plasmids MIJC20 and MITE17 were provided by the ABRC and introduced into *Escherichia coli* strain SW102 (Zhou et al., 2011). The GGGGGA-*m*Cherry(RFP)-3xFLAG-tag was introduced after nucleotide 29980 of MIJC20 and after nucleotide 60213 of MITE17. This generated *XylT* C-terminally fused to *m*Cherry and *BiP* with *m*Cherry inserted at −16 amino acids leaving the C-terminal HDEL signal intact for ER retention. The resulting genomic fragments with RFP (nucleotides 28704 to 34285 of MIJC20 for BiP-RFP and nucleotides 56288 to 61239 of MITE17 for XylT-RFP) were rescued in pENTR11DS (Life Technologies) to produce pEnBiP-RFP and pEnXylT-RFP, which were then recombined into pFAJGW using LR clonase (Life Technologies). pFAJ-BiP-RFP and pFAJ-XylT-RFP were introduced into *Agrobacterium tumefaciens* strain ABI (Cheng et al., 1997) for *Arabidopsis* transformation using a floral spray protocol (Chung et al., 2000).

Arabidopsis plants expressing SYP61-CFP were described previously (Robert et al., 2008) and provided by Drakakaki (University of California, Davis, CA). The SYP61-CFP transgene was introduced into GFP-KOR1 lines by genetic crosses. Markers for transient expression were RFP-SYP61 for the TGN (Lam et al., 2009), OFP-ER for the ER (Frank et al., 2008), and TPK1-RFP for tonoplasts (Batistic, 2012), originally described as GFP fusion (Maîtrejean et al., 2011).

Plant Transformation and Selection

The entry plasmids were recombined with pFAJGW (Feng et al., 2011) or pMDC99 using LR Clonase (Invitrogen) to generate a binary vector with phosphinothricin or hygromycin resistance. The resulting pFAJ-KOR1 and pMDC-KOR1 plasmids were introduced into *Agrobacterium* strain ABI or GV3101 for floral spray protocol (Chung et al., 2000). To select PPT^R transformants, seeds of dip-transformed plants were sown onto soil mix, and 5-d-old plants were sprayed with 30 μg/mL phosphinothricin solution. Hygromycin selection was conducted as described previously (Koiwa et al., 2003).

Transient Expression in *Arabidopsis* Protoplasts

Protoplasts were prepared from leaves of 4- to 5-week-old in vitro culture plants and transfected by the polyethylene glycol method as described previously (Frank et al., 2008). Routinely, 5×10^5 protoplasts were incubated with 30 μg of purified plasmid DNA (NucleoBond AX kits; Macherey-Nagel) premixed in a total volume of 50 μL TE buffer. Where indicated, 5 to 10 μM tunicamycin (dissolved in dimethylformamide; Serva) was included as *N*-glycosylation inhibitor.

Light Microscopy

Fluorescent signals were recorded by confocal laser scanning microscopy as described previously (Frank et al., 2008; Häweker et al., 2010) using either a Leica TCS SP2/AOBS, SP5/AOBS with HyD technology, or Olympus FV1000 (all equipped with an inverse objective lens setup and simultaneous multicolor detection).

Immunoblot Analyses

Protein extraction, PNGase-F treatment, SDS-PAGE, and blot transfer were performed essentially as described previously (Frank et al., 2008; Häweker et al., 2010). Antibodies used for immunoblotting were anticomplex glycan (PHA-L antigen) (Kaulfürst-Soboll et al., 2011), anti-GFP (Genscript), and anti-RGS-His (Qiagen).

GUS Staining

The seeds of the transgenic *Arabidopsis* line (Col-0) expressing GUS-KOR1 were germinated on 1× MS media supplemented with 3% sucrose and 1.5% agar. Seedlings were harvested on day 2 and day 12. For etiolation, seeds were germinated and kept in the dark for 6 d. GUS activity was detected in situ as described (Jefferson, 1987).

Purification of KOR1

The transgenic *Arabidopsis* line expressing RGS-His-KOR1 was provided by Simon Turner (University of Manchester, UK). A cell culture of this line was established and maintained in vitro on media containing 1× MS salts, 2% sucrose, 1× B5 vitamins, 0.2 g/L KH_2PO_4 1 mg/L 2,4-D, 0.05 mg/L kinetin, and 1% agar. The total membrane fraction was isolated as described by Borner et al. (2003) and resuspended in KOR extraction buffer (1% Nonidet P-40, 50 mM KH_2PO_4, pH 7.0, and 300 mM NaCl) containing 10 mM imidazole. After centrifugation at 10,000*g* for 10 min, 50 μL of Ni^{2+}-loaded IMAC Sepharose (GE Healthcare) suspended in 100 μL KOR1 extraction buffer was added and mixed by rotation at 4°C for 60 min. The slurry was loaded onto a centrifuge column (No. 69720; Pierce), and the resin was washed three times with 250 μL of extraction buffer containing 20 mM imidazole by successive centrifugation. Proteins were eluted from the resin with extraction buffer containing 250 mM imidazole in three 30-μL steps and concentrated by trichloroacetic acid precipitation.

2D-PAGE

2D-PAGE analysis was performed as described previously (Koiwa et al., 1994). The trichloroacetic acid-precipitated and dried RGS-His-KOR1 fraction was dissolved in sample buffer containing 8 M urea, 2% Nonidet P-40, and 2% ampholine and loaded onto the anode side of an isoelectric focusing (IEF) gel in a glass capillary (ϕ 1 mm) containing 2% ampholine (pH 3 to 10; GE Healthcare). The conditions for IEF were 100 V for 1 h (prerun), 100 V for 1 h, and 300 V for 3 h. After IEF, the capillary gel was equilibrated in 1× SDS-PAGE loading buffer and placed on top of a SDS-PAGE slab gel. The capillary gel was sealed by 1% agarose in 1× SDS-PAGE loading buffer before starting the second dimension run and subsequent blot transfer to a polyvinylidene fluoride membrane.

Accession Numbers

Sequence data from this article can be found in the GenBank/EMBL data libraries under accession numbers AAM63370.1, NP_176738.1, NP_199783.1, NP_194157.1, CAB51903.1, ABP96983.1, BAF30815.1, ACT54547.1, ABD62083.1, AAQ08018.1, AAS87601.1, AAP83128.1, BAA94257.1, AAC49704.1, ABD32918.1, NP_001050004.1, NP_001053204.1, NP_001051192.1, EAY94707.1, EEE58992.1, XP_001775325.1, XP_001772986.1, XP_001763929.1, XP_001759056.1, XP_001754846.1, ABR16291.1, ABR15471.1, AAT75041.1, AAS45400.1, XP_002332697.1, XP_002299405.1, XP_002312211.1, XP_002315101.1, BAF42036.1, BAC22690.1, XP_002519394.1, XP_002515321.1, XP_002514768.1, XP_002463915.1, XP_002465324.1, XP_002446733.1, AAM13693.1, CAN68337.1, XP_002266444.1, CAO15609.1, XP_002269783.1, ACR36366.1, ACG29946.1, NP_001147537.1, NP_001147970.1, NP_001151770.1, and ACN28577.1, and in the Arabidopsis Genome Initiative under accession numbers *STT3a*, At5g19690; *RSW2*/*KOR1*, At5g49720; *CGL1* (*GNTI*), At4g38240; *GNTII*, At2g05320; *FUCTA*, At3g19280; *FUCTB*, At1g49710; *XYLT*, At5g55500; *HGL1* (*MANII*), At5g14950; and *GALT1*, At1g26810.

Supplemental Data

The following materials are available in the online version of this article.

Supplemental Figure 1. Structure and Functionality of the KOR1 Complementation/Reporter Cassettes.

Supplemental Figure 2. Subcellular Localization of GFP-KOR1.

Supplemental Figure 3. Immunoblot Analyses of *rsw2-1* and *stt3a-2* Stably Transformed with *GFP-KOR1* Wild-Type or Variants Lacking *N*-Glycosylation Sites.

Supplemental Figure 4. *N*-Glycosylation of GFP-RSW2-1 Is Comparable to Wild-Type GFP-KOR1.

Supplemental Figure 5. Immunoblot Analyses of *rsw2-1* and *stt3a-2* Protoplasts Transfected with *GFP-KOR1* Wild-Type and Expression Cassettes with Mutated *N*-Glycosylation Sites.

Supplemental Figure 6. Additional Protoplast Images Obtained from the Experiment Described in Figure 8.

Supplemental Figure 7. Diversity of GFP-KOR1Δall Targeting.

Supplemental Figure 8. Two-Dimensional PAGE-Immunoblot Analysis of Affinity-Enriched RGS-His-KOR1 Protein.

Supplemental Figure 9. PNGase-F Treatment of *Arabidopsis* Extracts.

Supplemental Table 1. Oligonucleotide Primers Used in This Study.

ACKNOWLEDGMENTS

We thank Simon Turner (University of Manchester, UK) for donating the RGS-His-KOR1 construct plus seeds of transgenic plants, Georgia Drakakaki (UC Davis) for the SYP61-CFP construct/transgenic plants, Ping He (Texas A&M University) for the RFP-SYP61 plasmid, Kyun Oh Lee (Gyeongsang National University) for the *galT1-1* line, and Oliver Batistic (WWU Münster) for the TPK1-RFP construct. The *Arabidopsis* stock centers (ABRC and NASC) provided various T-DNA insertion lines and the Institut National de la Recherche Agronomique (Versailles, France) the *gnTII* mutant line. H.K. thanks Stanislav Vitha (Texas A&M University) for assistance in confocal microscopy. All authors thank Olessja Becker, Xiaoqiang Wu, Jun Qin, Sewon Kim, Meenu Vikram, and Edwin Mendez for technical assistance. This work was in part financially supported by Deutsche Forschungsgemeinschaft Grants SCHA 541/9 and 11 (to A.v.S.), by USDA-CSREES "Designing food for health" Grant 2010-34402-20875 (to H.K.), and by an Experiential Learning for Undergraduate research grant from Department of Horticultural Sciences, Texas A&M University (to H.K. and J.L.W.).

AUTHOR CONTRIBUTIONS

A.v.S. and H.K. designed experiments. S.R., N.B., I.S.J., J.L.W., A.v.S., and H.K. performed research. S.R., A.v.S., and H.K. analyzed data. S.R., A.v.S., and H.K. wrote the article.

Received July 9, 2014; revised August 14, 2014; accepted September 9, 2014; published September 19, 2014.

REFERENCES

Adney, W.S., Jeoh, T., Beckham, G.T., Chou, Y.C., Baker, J.O., Michener, W., Brunecky, R., and Himmel, M.E. (2009). Probing the role of N-linked glycans in the stability and activity of fungal cellobiohydrolases by mutational analysis. Cellulose **16:** 699–709.

Arnold, K., Bordoli, L., Kopp, J., and Schwede, T. (2006). The SWISS-MODEL workspace: a web-based environment for protein structure homology modelling. Bioinformatics **22:** 195–201.

Barre, A., Herve, C., Lescure, B., and Rouge, P. (2002). Lectin receptor kinases in plants. Crit. Rev. Plant Sci. **21:** 379–399.

Bashline, L., Li, S., Anderson, C.T., Lei, L., and Gu, Y. (2013). The endocytosis of cellulose synthase in Arabidopsis is dependent on μ2, a clathrin-mediated endocytosis adaptin. Plant Physiol. **163:** 150–160.

Batistic, O. (2012). Genomics and localization of the Arabidopsis DHHC-cysteine-rich domain S-acyltransferase protein family. Plant Physiol. **160:** 1597–1612.

Borner, G.H., Lilley, K.S., Stevens, T.J., and Dupree, P. (2003). Identification of glycosylphosphatidylinositol-anchored proteins in Arabidopsis. A proteomic and genomic analysis. Plant Physiol. **132:** 568–577.

Cheng, M., Fry, J.E., Pang, S., Zhou, H., Hironaka, C.M., Duncan, D.R., Conner, T.W., and Wan, Y. (1997). Genetic transformation of wheat mediated by *Agrobacterium tumefaciens.* Plant Physiol. **115:** 971–980.

Chung, M.-H., Chen, M.-K., and Pan, S.-M. (2000). Floral spray transformation can efficiently generate Arabidopsis transgenic plants. Transgenic Res. **9:** 471–476.

Collings, D.A., Gebbie, L.K., Howles, P.A., Hurley, U.A., Birch, R.J., Cork, A.H., Hocart, C.H., Arioli, T., and Williamson, R.E. (2008). Arabidopsis dynamin-like protein DRP1A: a null mutant with widespread defects in endocytosis, cellulose synthesis, cytokinesis, and cell expansion. J. Exp. Bot. **59:** 361–376.

Drakakaki, G., van de Ven, W., Pan, S., Miao, Y., Wang, J., Keinath, N.F., Weatherly, B., Jiang, L., Schumacher, K., Hicks, G., and Raikhel, N. (2012). Isolation and proteomic analysis of the SYP61 compartment reveal its role in exocytic trafficking in Arabidopsis. Cell Res. **22:** 413–424.

Feng, Y., Cao, C.M., Vikram, M., Park, S., Kim, H.J., Hong, J.C., Cisneros-Zevallos, L., and Koiwa, H. (2011). A three-component gene expression system and its application for inducible flavonoid overproduction in transgenic *Arabidopsis thaliana*. PLoS ONE **6:** e17603.

Fitchette-Lainé, A.C., Gomord, V., Cabanes, M., Michalski, J.C., Saint Macary, M., Foucher, B., Cavelier, B., Hawes, C., Lerouge, P., and Faye, L. (1997). N-glycans harboring the Lewis a epitope are expressed at the surface of plant cells. Plant J. **12:** 1411–1417.

Frank, J., Kaulfürst-Soboll, H., Rips, S., Koiwa, H., and von Schaewen, A. (2008). Comparative analyses of Arabidopsis *complex glycan1* mutants and genetic interaction with *staurosporin and temperature sensitive3a*. Plant Physiol. **148:** 1354–1367.

Guex, N., and Peitsch, M.C. (1997). SWISS-MODEL and the Swiss-PdbViewer: an environment for comparative protein modeling. Electrophoresis **18:** 2714–2723.

Häweker, H., Rips, S., Koiwa, H., Salomon, S., Saijo, Y., Chinchilla, D., Robatzek, S., and von Schaewen, A. (2010). Pattern recognition receptors require N-glycosylation to mediate plant immunity. J. Biol. Chem. **285:** 4629–4636.

Helenius, A., and Aebi, M. (2001). Intracellular functions of N-linked glycans. Science **291:** 2364–2369.

Hématy, K., Sado, P.E., Van Tuinen, A., Rochange, S., Desnos, T., Balzergue, S., Pelletier, S., Renou, J.P., and Höfte, H. (2007). A receptor-like kinase mediates the response of Arabidopsis cells to the inhibition of cellulose synthesis. Curr. Biol. **17:** 922–931.

Jefferson, R. (1987). Assaying chimeric genes in plants: The GUS gene fusion system. Plant Mol. Biol. Rep. **5:** 387–405.

Johnson, K.D., and Chrispeels, M.J. (1987). Substrate specificities of N-acetylglucosaminyl-, fucosyl-, and xylosyltransferases that modify glycoproteins in the Golgi apparatus of bean cotyledons. Plant Physiol. **84:** 1301–1308.

Jung, E.D., Lao, G., Irwin, D., Barr, B.K., Benjamin, A., and Wilson, D.B. (1993). DNA sequences and expression in Streptomyces lividans of an exoglucanase gene and an endoglucanase gene from *Thermomonospora fusca*. Appl. Environ. Microbiol. **59:** 3032–3043.

Kajiura, H., Koiwa, H., Nakazawa, Y., Okazawa, A., Kobayashi, A., Seki, T., and Fujiyama, K. (2010). Two *Arabidopsis thaliana* Golgi

alpha-mannosidase I enzymes are responsible for plant N-glycan maturation. Glycobiology **20:** 235–247.

Kang, J.S., et al. (2008). Salt tolerance of *Arabidopsis thaliana* requires maturation of N-glycosylated proteins in the Golgi apparatus. Proc. Natl. Acad. Sci. USA **105:** 5933–5938.

Kaulfürst-Soboll, H., Rips, S., Koiwa, H., Kajiura, H., Fujiyama, K., and von Schaewen, A. (2011). Reduced immunogenicity of Arabidopsis hybrid glycosylation1 (hgl1) N-glycans due to altered accessibility of xylose and core fucose epitopes. J. Biol. Chem. **286:** 22955–22964.

Kayser, V., Chennamsetty, N., Voynov, V., Forrer, K., Helk, B., and Trout, B.L. (2011). Glycosylation influences on the aggregation propensity of therapeutic monoclonal antibodies. Biotechnol. J. **6:** 38–44.

Kelleher, D.J., Karaoglu, D., Mandon, E.C., and Gilmore, R. (2003). Oligosaccharyltransferase isoforms that contain different catalytic STT3 subunits have distinct enzymatic properties. Mol. Cell **12:** 101–111.

Khademi, S., Guarino, L.A., Watanabe, H., Tokuda, G., and Meyer, E.F. (2002). Structure of an endoglucanase from termite, *Nasutitermes takasagoensis*. Acta Crystallogr. D Biol. Crystallogr. **58:** 653–659.

Koiwa, H., Sato, F., and Yamada, Y. (1994). Characterization of accumulation of tobacco PR-5 proteins by IEF-immunoblot analysis. Plant Cell Physiol. **35:** 821–827.

Koiwa, H., Li, F., McCully, M.G., Mendoza, I., Koizumi, N., Manabe, Y., Nakagawa, Y., Zhu, J., Rus, A., Pardo, J.M., Bressan, R.A., and Hasegawa, P.M. (2003). The STT3a subunit isoform of the Arabidopsis oligosaccharyltransferase controls adaptive responses to salt/osmotic stress. Plant Cell **15:** 2273–2284.

Lam, S.K., Cai, Y., Tse, Y.C., Wang, J., Law, A.H., Pimpl, P., Chan, H.Y., Xia, J., and Jiang, L. (2009). BFA-induced compartments from the Golgi apparatus and trans-Golgi network/early endosome are distinct in plant cells. Plant J. **60:** 865–881.

Lane, D.R., et al. (2001). Temperature-sensitive alleles of RSW2 link the KORRIGAN endo-1,4-beta-glucanase to cellulose synthesis and cytokinesis in Arabidopsis. Plant Physiol. **126:** 278–288.

Laurière, M., Laurière, C., Chrispeels, M.J., Johnson, K.D., and Sturm, A. (1989). Characterization of a xylose-specific antiserum that reacts with the complex asparagine-linked glycans of extracellular and vacuolar glycoproteins. Plant Physiol. **90:** 1182–1188.

Lehle, L., Strahl, S., and Tanner, W. (2006). Protein glycosylation, conserved from yeast to man: a model organism helps elucidate congenital human diseases. Angew. Chem. Int. Ed. Engl. **45:** 6802–6818.

Lei, L., Zhang, T., Strasser, R., Lee, C.M., Gonneau, M., Mach, L., Vernhettes, S., Kim, S.H., J Cosgrove, D., Li, S., and Gu, Y. (2014). The jiaoyao1 mutant is an allele of korrigan1 that abolishes endoglucanase activity and affects the organization of both cellulose microfibrils and microtubules in Arabidopsis. Plant Cell **26:** 2601–2616.

Léonard, R., Costa, G., Darrambide, E., Lhernould, S., Fleurat-Lessard, P., Carlué, M., Gomord, V., Faye, L., and Maftah, A. (2002). The presence of Lewis a epitopes in *Arabidopsis thaliana* glycoconjugates depends on an active alpha4-fucosyltransferase gene. Glycobiology **12:** 299–306.

Liebminger, E., Grass, J., Altmann, F., Mach, L., and Strasser, R. (2013). Characterizing the link between glycosylation state and enzymatic activity of the endo-β1,4-glucanase KORRIGAN1 from *Arabidopsis thaliana*. J. Biol. Chem. **288:** 22270–22280.

Liebminger, E., Veit, C., Pabst, M., Batoux, M., Zipfel, C., Altmann, F., Mach, L., and Strasser, R. (2011). Beta-N-acetylhexosaminidases HEXO1 and HEXO3 are responsible for the formation of paucimannosidic N-glycans in *Arabidopsis thaliana*. J. Biol. Chem. **286:** 10793–10802.

Liebminger, E., Hüttner, S., Vavra, U., Fischl, R., Schoberer, J., Grass, J., Blaukopf, C., Seifert, G.J., Altmann, F., Mach, L., and Strasser, R. (2009). Class I alpha-mannosidases are required for N-glycan processing and root development in *Arabidopsis thaliana*. Plant Cell **21:** 3850–3867.

Maîtrejean, M., Wudick, M.M., Voelker, C., Prinsi, B., Mueller-Roeber, B., Czempinski, K., Pedrazzini, E., and Vitale, A. (2011). Assembly and sorting of the tonoplast potassium channel AtTPK1 and its turnover by internalization into the vacuole. Plant Physiol. **156:** 1783–1796.

Master, E.R., Rudsander, U.J., Zhou, W., Henriksson, H., Divne, C., Denman, S., Wilson, D.B., and Teeri, T.T. (2004). Recombinant expression and enzymatic characterization of PttCel9A, a KOR homologue from *Populus tremula* x *tremuloides*. Biochemistry **43:** 10080–10089.

Nebenführ, A., Gallagher, L.A., Dunahay, T.G., Frohlick, J.A., Mazurkiewicz, A.M., Meehl, J.B., and Staehelin, L.A. (1999). Stop-and-go movements of plant Golgi stacks are mediated by the acto-myosin system. Plant Physiol. **121:** 1127–1142.

Ni, M., Cui, D., Einstein, J., Narasimhulu, S., Vergara, C.E., and Gelvin, S.B. (1995). Strength and tissue specificity of chimeric promoters derived from the octopine and mannopine synthase genes. Plant J. **7:** 661–676.

Nicol, F., His, I., Jauneau, A., Vernhettes, S., Canut, H., and Höfte, H. (1998). A plasma membrane-bound putative endo-1,4-beta-D-glucanase is required for normal wall assembly and cell elongation in Arabidopsis. EMBO J. **17:** 5563–5576.

Oliver, J.D., van der Wal, F.J., Bulleid, N.J., and High, S. (1997). Interaction of the thiol-dependent reductase ERp57 with nascent glycoproteins. Science **275:** 86–88.

Pedrazzini, E., Komarova, N.Y., Rentsch, D., and Vitale, A. (2013). Traffic routes and signals for the tonoplast. Traffic **14:** 622–628.

Peng, L., Kawagoe, Y., Hogan, P., and Delmer, D. (2002). Sitosterol-beta-glucoside as primer for cellulose synthesis in plants. Science **295:** 147–150.

Rath, A., Glibowicka, M., Nadeau, V.G., Chen, G., and Deber, C.M. (2009). Detergent binding explains anomalous SDS-PAGE migration of membrane proteins. Proc. Natl. Acad. Sci. USA **106:** 1760–1765.

Robert, S., Chary, S.N., Drakakaki, G., Li, S., Yang, Z., Raikhel, N.V., and Hicks, G.R. (2008). Endosidin1 defines a compartment involved in endocytosis of the brassinosteroid receptor BRI1 and the auxin transporters PIN2 and AUX1. Proc. Natl. Acad. Sci. USA **105:** 8464–8469.

Robert, S., Bichet, A., Grandjean, O., Kierzkowski, D., Satiat-Jeunemaître, B., Pelletier, S., Hauser, M.T., Höfte, H., and Vernhettes, S. (2005). An Arabidopsis endo-1,4-beta-D-glucanase involved in cellulose synthesis undergoes regulated intracellular cycling. Plant Cell **17:** 3378–3389.

Roudier, F., Fernandez, A.G., Fujita, M., Himmelspach, R., Borner, G.H., Schindelman, G., Song, S., Baskin, T.I., Dupree, P., Wasteneys, G.O., and Benfey, P.N. (2005). COBRA, an Arabidopsis extracellular glycosyl-phosphatidyl inositol-anchored protein, specifically controls highly anisotropic expansion through its involvement in cellulose microfibril orientation. Plant Cell **17:** 1749–1763.

Rozwadowski, K., Yang, W., and Kagale, S. (2008). Homologous recombination-mediated cloning and manipulation of genomic DNA regions using Gateway and recombineering systems. BMC Biotechnol. **8:** 88.

Ruiz-Canada, C., Kelleher, D.J., and Gilmore, R. (2009). Cotranslational and posttranslational N-glycosylation of polypeptides by distinct mammalian OST isoforms. Cell **136:** 272–283.

Samson, F., Brunaud, V., Balzergue, S., Dubreucq, B., Lepiniec, L., Pelletier, G., Caboche, M., and Lecharny, A. (2002). FLAGdb/FST: a database of mapped flanking insertion sites (FSTs) of *Arabidopsis thaliana* T-DNA transformants. Nucleic Acids Res. **30:** 94–97.

Schwede, T., Kopp, J., Guex, N., and Peitsch, M.C. (2003). SWISS-MODEL: An automated protein homology-modeling server. Nucleic Acids Res. **31:** 3381–3385.

Silberstein, S., and Gilmore, R. (1996). Biochemistry, molecular biology, and genetics of the oligosaccharyltransferase. FASEB J. **10:** 849–858.

Skropeta, D. (2009). The effect of individual N-glycans on enzyme activity. Bioorg. Med. Chem. **17:** 2645–2653.

Stefanowicz, K., Lannoo, N., Proost, P., and Van Damme, E.J. (2012). Arabidopsis F-box protein containing a Nictaba-related lectin domain interacts with N-acetyllactosamine structures. FEBS Open Bio **2:** 151–158.

Strasser, R., Altmann, F., Mach, L., Glössl, J., and Steinkellner, H. (2004). Generation of *Arabidopsis thaliana* plants with complex N-glycans lacking beta1,2-linked xylose and core alpha1,3-linked fucose. FEBS Lett. **561:** 132–136.

Strasser, R., Schoberer, J., Jin, C., Glössl, J., Mach, L., and Steinkellner, H. (2006). Molecular cloning and characterization of *Arabidopsis thaliana* Golgi alpha-mannosidase II, a key enzyme in the formation of complex N-glycans in plants. Plant J. **45:** 789–803.

Strasser, R., Steinkellner, H., Borén, M., Altmann, F., Mach, L., Glössl, J., and Mucha, J. (1999). Molecular cloning of cDNA encoding N-acetylglucosaminyltransferase II from *Arabidopsis thaliana*. Glycoconj. J. **16:** 787–791.

Strasser, R., Mucha, J., Mach, L., Altmann, F., Wilson, I.B., Glössl, J., and Steinkellner, H. (2000). Molecular cloning and functional expression of beta1, 2-xylosyltransferase cDNA from *Arabidopsis thaliana*. FEBS Lett. **472:** 105–108.

Strasser, R., Bondili, J.S., Schoberer, J., Svoboda, B., Liebminger, E., Glössl, J., Altmann, F., Steinkellner, H., and Mach, L. (2007a). Enzymatic properties and subcellular localization of Arabidopsis beta-N-acetylhexosaminidases. Plant Physiol. **145:** 5–16.

Strasser, R., Bondili, J.S., Vavra, U., Schoberer, J., Svoboda, B., Glössl, J., Léonard, R., Stadlmann, J., Altmann, F., Steinkellner, H., and Mach, L. (2007b). A unique beta1,3-galactosyltransferase is indispensable for the biosynthesis of N-glycans containing Lewis a structures in *Arabidopsis thaliana*. Plant Cell **19:** 2278–2292.

Szyjanowicz, P.M., McKinnon, I., Taylor, N.G., Gardiner, J., Jarvis, M.C., and Turner, S.R. (2004). The irregular xylem 2 mutant is an allele of korrigan that affects the secondary cell wall of *Arabidopsis thaliana*. Plant J. **37:** 730–740.

Takahashi, J., et al. (2009). KORRIGAN1 and its aspen homolog PttCel9A1 decrease cellulose crystallinity in Arabidopsis stems. Plant Cell Physiol. **50:** 1099–1115.

Vain, T., Crowell, E.F., Timpano, H., Biot, E., Desprez, T., Mansoori, N., Trindade, L.M., Pagant, S., Robert, S., Höfte, H., Gonneau, M., and Vernhettes, S. (2014). The cellulase KORRIGAN is part of the cellulose synthase complex. Plant Physiol. **165:** 1521–1532.

Varki, A. (2011). Evolutionary forces shaping the Golgi glycosylation machinery: why cell surface glycans are universal to living cells. Cold Spring Harb. Perspect. Biol. **3:** 3.

Vembar, S.S., and Brodsky, J.L. (2008). One step at a time: endoplasmic reticulum-associated degradation. Nat. Rev. Mol. Cell Biol. **9:** 944–957.

von Schaewen, A., Frank, J., and Koiwa, H. (2008). Role of plant complex N-glycans. Plant Signal. Behav. **3:** 871–873.

von Schaewen, A., Sturm, A., O'Neill, J., and Chrispeels, M.J. (1993). Isolation of a mutant Arabidopsis plant that lacks N-acetyl glucosaminyl transferase I and is unable to synthesize Golgi-modified complex N-linked glycans. Plant Physiol. **102:** 1109–1118.

Voutilainen, S.P., Murray, P.G., Tuohy, M.G., and Koivula, A. (2010). Expression of *Talaromyces emersonii* cellobiohydrolase Cel7A in Saccharomyces cerevisiae and rational mutagenesis to improve its thermostability and activity. Protein Eng. Des. Sel. **23:** 69–79.

Xu, S.L., Rahman, A., Baskin, T.I., and Kieber, J.J. (2008). Two leucine-rich repeat receptor kinases mediate signaling, linking cell wall biosynthesis and ACC synthase in Arabidopsis. Plant Cell **20:** 3065–3079.

Zhou, R., Benavente, L.M., Stepanova, A.N., and Alonso, J.M. (2011). A recombineering-based gene tagging system for Arabidopsis. Plant J. **66:** 712–723.

Zuo, J., Niu, Q.W., Nishizawa, N., Wu, Y., Kost, B., and Chua, N.H. (2000). KORRIGAN, an Arabidopsis endo-1,4-beta-glucanase, localizes to the cell plate by polarized targeting and is essential for cytokinesis. Plant Cell **12:** 1137–1152.